TAMPERE UNIVERSITY OF TECHNOLOGY

ANTTI LAMBERG

CURVATURE EFFECTS IN LIPOPROTEIN FUSION

Master of Science Thesis

Examiner: Prof. Ilpo Vattulainen
Examiner and topic approved in
Science and Environmental Engineering
Faculty Council meeting on 6 June 2010

ABSTRACT

TAMPERE UNIVERSITY OF TECHNOLOGY
Master's Degree Programme in Science and Engineering
LAMBERG, ANTTI: Curvature Effects in Lipoprotein Fusion
Master of Science Thesis, 51 pages, 6 appendix pages
August 2011
Major: Physics
Examiner: Prof. Ilpo Vattulainen
Keywords: lipoprotein, fusion, coalescence, molecular dynamics, interfacial tension, elasticity

High and low density lipoproteins (HDL and LDL, respectively) are of tantamount interest to studies on human health, as these cholesterol transporters are highly involved in cardiovascular diseases, the leading cause of death in the industrialized world. While HDL acts to prevent cholesterol from building up in excess, the larger LDL particles may get stuck inside artery walls, fuse with other LDL particles and finally burst out from the wall, causing a stroke.

The fusion of simpler systems has been studied for decades, but the details of lipoprotein fusion and the factors promoting fusion remain elusive. In this Thesis we studied the effect of varying surfactant composition to lipid droplet fusion, which form the core of lipoproteins.

Pressure profiles have been suggested to give a quantitative picture of how properties of interfaces, such as interfacial tension arise. These profiles have been studied by physicists for a long time, but it was only relatively recently that a biological relevance was postulated and a new interest surged. While experimental techniques are still not refined enough to probe these biological systems because of their extremely small sizes, in the last few years it has become computationally feasible to carry out research in relevant length and time scales.

Using pressure profile calculations, we vary the surfactant compositions of HDL/LDL based lipid droplets so as to keep some quantities constant while varying others. From simple systems, it is known that interfacial tension is the most important factor in fusion and phase separation. Using large-scale computers to run a steered molecular dynamics simulation method developed by us, we show that the fusion rates of lipid droplets are greatly affected by their lipid composition and that interfacial tension alone cannot explain this tendency. We explore alternative explanations and their feasibility.

TIIVISTELMÄ

TAMPEREEN TEKNILLINEN YLIOPISTO
Teknis-luonnontieteellinen koulutusohjelma
LAMBERG, ANTTI: Curvature Effects in Lipoprotein Fusion
Diplomityö, 51 sivua, 6 liitesivua
Elokuu 2011
Pääaine: Fysiikka
Tarkastajat: Prof. Ilpo Vattulainen
Avainsanat: lipoproteiini, fuusio, molekyylidynamiikka, pintajännitys, elastisuus

Kansankielellä hyväksi kolesteroliksi kutsuttu HDL ja vastaavasti pahaksi kolesteroliksi kutsuttu LDL ovat nykylääketieteessä tärkeitä indikaattoreita yksilön yleisterveydestä. Nämä kaksi lipoproteiinia ovat vastuussa kolesterolin kuljettamisesta elimistön sisällä ja häiriöt näiden kierrossa ovat syy sydän- ja verisuonitauteihin, jotka ovat teollistuneissa maissa yleisin kuolinsyy. HDL kuljettaa kolesterolia kudoksista maksaan, mutta isompi LDL saattaa jäädä kiinni valtimoiten seinämiin, fuusioitua, eli yhdistyä, muiden LDL kanssa ja lopulta seinämän revetessä aiheuttaa tukkeuman.

Yksinkertaisempien systeemien fuusiota on tutkittu vuosikymmeniä, mutta prosessin yksityiskohdat ja siihen vaikuttavat tekijät ovat edelleen epäselviä. Tässä diplomityössä selvitetään HDL ja LDL perustuvien lipididroplettien pintakomponentin muuttamisen vaikutusta fuusioon.

Paineprofiilien on kirjallisuudessa ehdotettu kuvaavan sitä, miten pinnan fysikaaliset suureet, kuten pintajännitys, mekaanisesti syntyvät. Fyysikot ovat tutkineet näitä profiileita jo vuosikymmeniä, usein yksinkertaisille systeemeille, mutta vasta lähiaikoina niiden on ehdotettu olevan tärkeässä asemassa monimutkaisissa biologisissa prosesseissa. Koska mittakaava paineprofiileissa on niin pieni, on laboratoriokokeita vaikea tehdä, mutta kiitos viimeaikaisen tietokonekehityksen, on nykyään mahdollista tehdä numeerisia kokeita ja simulaatioita tietokoneilla.

Käyttäen paineprofiililaskuja, tässä diplomityössä muutettiin HDL/LDL:än perustuvien lipididroplettien pinta-aktiivisten molekyylien koostumusta pitäen fysikaalisia suureita vakiona. Yksinkertaisille systeemeille tiedetään pintajännityksen olevan tärkein tekijä faasiseparaatiossa ja fuusiossa. Käyttäen supertietokoneluokan tietokoneita molekyylidynamiikkasimulaatioiden ajamiseen, tässä diplomityössä näytetään lipidien koostumuksella olevan suuri vaikutus lipididroplettien fuusionopeuksiin, ja että pintajännitys yksinään ei pysty selittämään tätä eroa. Työssä esitetään vaihtoehtoisia syitä ja tutkitaan niiden soveltuvuutta.

PREFACE

The research for this Master of Science Thesis was conducted in the Biological Physics and Soft Matter Group of Prof. Ilpo Vattulainen in Tampere University of Technology using the computing resources of CSC — IT Center for Science.

First and foremost I wish to thank Dr. Samuli Ollila, who for the past few years has been a personal friend and mentor of mine. This Thesis was inspired by his ideas and previous work on the field as well as his continuous input as I was working on the Thesis. As he is no longer at TUT, I wish him all the best and I do hope to collaborate with him in the future as well.

This project would not have been possible without Prof. Ilpo Vattulainen, who put a great deal of trust into me, even as the work was considerably delayed. He furthermore granted great freedom and independence to pursue my own interests in this Thesis all the while making sure that these interests were also of scientific relevance. For all this, I would like to express my sincerest gratitude to Prof. Vattulainen.

I wish extend my expressions of gratitude to the rest of the group members as well, both for scientific discussions and for arranging numerous extracurricular activities to keeo the mind fresh. Especially Matti and Hector, who entered the research group in Tampere around the same time as I did, were always willing to listen to and to help me with my problems and to spend time together. I am also indebted to countless other people, particularly friends for helping me during times of need, but regrettably the list is too long to be written down. For those who recognize themselves from this description, thank you.

Last, but not least, I am grateful to my parents for their continued support throughout my studies.

Now, new challenges await, さよなら。

Tampere, August 2011

Antti Lamberg

CONTENTS

NOTATION AND ABBREVIATIONS

A	Interfacial Area
a	Thickness of Stalk
c_0	Spontaneous Curvature
$\mathbf{e}$	Basis Vector
F	Helmholtz Free Energy
$\mathbf{F}$	Force
g_{ij}	Metric Tensor
H	Mean Curvature
$\mathcal{H}$	Hamiltonian
K	Gaussian Curvature
$\mathcal{K}$	Kinetic Energy
k	Bending Modulus
$\bar{k}$	Gaussian Bending Modulus
ℓ	Lenght of Spring
P	Bulk Pressure
P_{ij}	Pressure Tensor
P_T	Tangential Component of Pressure
P_N	Normal Component of Pressure
R	Physical Radius
r	Radius
$\mathbf{r}$	Position
r_s	Laplace's Radius
S	Entropy
T	Temperature
$U^{(m)}$	m-body Potential
V	Volume
$\mathbf{v}$	Velocity
Z	Partition Function
α, β	Phases
δ	Dirac Distribution
Δt	Time-step
ε_{ij}	Strain Tensor
Φ	Interparticle Potential
σ	Interfacial Tension
σ_s	Surface Tension at Laplace's Radius
σ_{ij}	Stress Tensor
ω	Solid Angle

CHOL	Cholesterol
CG	Coarse-Grained
HDL	High Density Lipoprotein
LDL	Low Density Lipoprotein
lysoPC	Lysophosphatidylcholine
MD	Molecular Dynamics
POPC	Phosphatidylcholine
SCFT	Self Consistent Field Theory
TRIOL	Trioleate

1. INTRODUCTION

High and low density lipoproteins (HDL and LDL, respectively) are biological particles of immense interest to modern medicine. The amount of lipoproteins, or cholesterol as they are often referred to, in the blood stream has been found to strongly correlate with the risk of cardiovascular disease, the leading cause of death in the western world. High concentrations of HDL have been found to lower the risk of atherosclerosis, whereas LDL has the opposite effect. These particles are often referred to as the good and the bad cholesterol [1].

Atherosclerosis is the condition in which the arteries clog due to a build-up of fatty materials. The condition is worsened by aggregation and fusion of LDL particles inside the artery walls. Furthermore, it has been experimentally shown that by changing the surface composition of lipoproteins, one can affect their aggregation and fusion [2]. The mechanism, however, is not fully understood. In this work our goal is to study which surface properties of the particles determine their tendency to fuse and how these properties depend on molecular composition at the surface.

Based on predictions on a well-established continuum mechanical elastic model of lipoprotein fusion originally developed by Markin *et al.* [3], we alter the composition of lipoproteins and run molecular scale numerical simulations. The aforementioned model proposes that by changing a property called spontaneous curvature, which is roughly speaking the ratio of the size of the head group and the size of the tail of a surfactant molecule, we may alter the fusion rate. Because the model in question is a continuum model and is originally developed for small curvatures in bilayers, it is not at all clear that its predictions should hold for a monolayer system in high curvature regions. Although we cannot expect quantitative correspondence between the continuum theory and computer simulations for several reasons to be outlined later, there might be a qualitative truth to the theory even in small scales. This is what we set out to study by means of molecular dynamics.

Although there have been previous similar computational studies of related systems [4], the present work is to the author's knowledge the first study to use a system with biologically relevant compositions and forcefields. This is due to the fact that only very recently has it become feasible to use computer simulations for semi-quantitative predictions in the size- and timescales relevant to biological phenomena. This in turn is due in part to recent developments in numerical tools and the parametrization of

models based on experimental results. All of the above is enabled by the ongoing massive increase in computer system performance.

Using computer simulations of lipoparticles stripped of their constituent proteins, we found out that the surfactant composition affects fusion of such emulsion droplets not only through modifying surface tension, but clearly also by changing elastic curvature constants, most strikingly spontaneous curvature.

2. BIOLOGICAL OVERVIEW

In this short Chapter, we discuss the biological motivation of this work as well as the essentials of related biochemistry. We review the chemical formulas of the constituents of the HDL and LDL particles. We then proceed to consider some recent experimental results and briefly discuss their relevance to the present study. For a thorough reiw on lipoproteins, see e.g. Ref. [1].

2.1 Lipids, Membranes and Lipoproteins in a Nutshell

Lipids are a broad group of biologically relevant materials that are characterized by solubility. A lipid is defined as a member of a group of compounds that are insoluble in water, but soluble in nonpolar solvents [5]. Typically then, a lipid has both a hydrophilic and a hydrophobic end. They self-assemble and form membranes and droplets, which make up the critical components of many biological objects.

For example, cellular membranes are bilayers, i.e. they are made up of two layers of lipids in such a way that the hydrophobic ends are shielded from water, see Fig. 2.1. Another example is a lipid droplet, where a hydrophobic core, consisting of e.g. triglycerides. is surrounded by a phospholipid monolayer. In chemical engineering, objects of this kind are called emulsion particles. Lipid droplets become relevant in a biological context when they absorb a protein on their surface or as a reservoir of fats.

The surface of the HDL and LDL droplets are made up of cholesterol and phospholipids: phosphatidylcholine, lysophosphatidylcholine, sphingomyelin, phosphatidyketanolamine, diasylglycerol and ceramide. The core of the droplets is mainly cholesterol oleyl esther and triglyceride. The chemical compositions of these particles are illustrated in Fig. 2.2. Furthermore, HDL accomodates from one to three Apo-A1 proteins on its surface, while on LDL there's only one protein called Apo-B100. The radius of LDL is about 5–10 nm, making it roughly twice the size of HDL.

2.2 Relevance of Lipoparticles to Biological Function

The primary task of LDL and HDL is to act as cholesterol transporters, carrying it into and out of cells, respectively. LDL is often referred to as bad cholesterol, for it is these particles that exit the blood stream as they penetrate into the walls of arteries. They might get stuck within the walls and undergo chemical reactions,

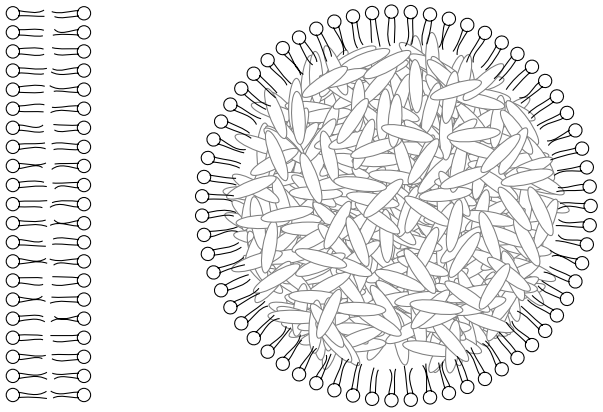

Lipid bilayer Lipid droplet

Figure 2.1: Schematic illustrations of the system types discussed in this Thesis.

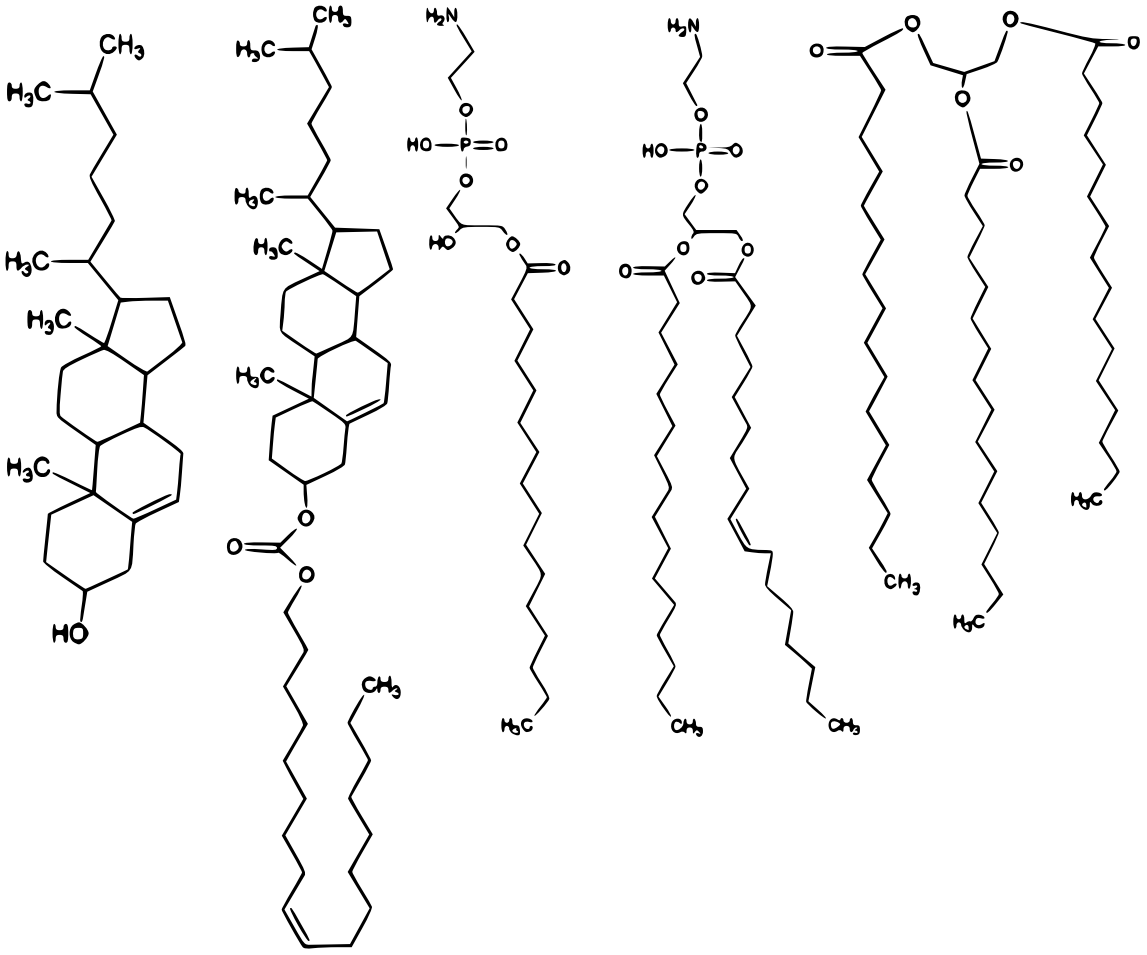

Figure 2.2: Illustrations of the molecules discussed in this Thesis: (from the left) cholesterol, cholesterol oleyl esther, lysophosphatidylcholine, phosphatidylcholine, triglyceride.

which makes them prone to fuse and finally to form so-called foam. If this foam grows large enough, the artery wall might rupture inwards and a blood clog might form. This in turn is an immediate health hazard, as it may lead to a stroke or to a cardiac arrest [1].

HDL particles, or the good cholesterol, also enter the artery walls but do not get stuck there due to their small size. Rather, they transport the material formed by LDL fusion away, thus preventing the aforementioned pathological conditions. From these considerations, it is of little surprise that low levels of HDL and high levels of LDL are strongly correlated with the risk of cardiovascular disease.

Strictly speaking, lipoproteins are divided into five categories, of which chylomicrons represent the biggest particles. These are formed from digested food in the small intestine. They are then secreted into the bloodstream where they transport fatty acids to muscle cells and finally end their cycle in the liver. VLDLs (very low density lipoproteins) are formed in the liver from the remnants of chylomicrons and transport cholesterol and triglyceride to cells. Encountering the lipoprotein lipase enzyme, VLDLs are, through an intermediate stage called IDL (intermediate density lipoprotein), transformed to LDLs. The main purpose of the particles as transporters of cholesterol and triglyceride remain the same all through their life cycle, although the body does have receptors to distinguish between the different life stages, namely VLDL-IDL-LDL.

In contrast to LDL, HDL is formed directly in the liver from Apo-A1 proteins and phospholipids. Initially they start out as discoidal particles, but as their main purpose is to collect cholesterol from the cells back to the bloodstream, they quickly become round. There are several different mechanisms to further transport the excess cholesterol out from the HDL.

3. THEORETICAL CONCEPTS

In this Chapter we give a brief overview of the theoretical concepts and physical quantities used in this Thesis.

In Section 3.1 we review the thermodynamics of surface tension of spherical particles. In terms of understanding the fusion rates of lipoparticles this property is of central importance, since it is well known that macrophase of emulsion particles becomes less stable as the surface tension is increased. Furthermore, surface tension has importance as a way of model verification, since it can be routinely measured for macroscopic systems. Once we have developed the notion of pressure profiles, we may link the concept of surface tension to a more mechanical one, a route which is more convenient from a computational point of view. The treatment from a mechanical point of view is described later, in Section 3.3.

The concept of local pressure, as a generalization of the notion of pressure, is introduced in Section 3.2. Computationally it provides a convenient tool to calculate the surface tension of complex systems. In addition, it gives insight into how surface tension, a macroscopic property, arises from microscopic interactions and when it indeed is a good characterization of the system under study, as shown in Section 3.3.

Section 3.4 gives a brief overview of the relevant parts of the theory of continuum elasticity. This Section formalizes the qualitative discussion of Section 3.2. It is important to note that the definitions used in the aforementioned Section deviate from the customary ones. Rather than taking pressure as the quantity whose divergence is the force density, we define pressure in terms of derivatives of the free energy. This subtle change turns out to be of fundamental importance as it is said to guarantee the uniqueness of the pressure tensor, which has been a heated topic for quite some time. To achieve these goals, we rely heavily on tensor calculus. We have therefore provided a short list of the properties of tensors as an appendix.

Finally, in Section 3.5 we give a simple justification for the Helfrich elasticity theory, which in essence is a continuum model for bilayer elasticity. Later, in Chapter 4, we develop the lipoprotein fusion model that is based on the results of this Section. Although we discuss about a model of lipoprotein fusion based on the Helfrich theory, it is important to realize that due to some approximations this may not be a applicable to our problem. Therefore it is necessary to be aware of the approximations involved in the Helfrich theory.

3.1 Interfacial Tension

Interfacial, or surface, tension is the surface energy density associated to an interface. More precisely, it is the energy density difference of a system with an interface and the same system consisting of just its bulk phases. Thus surface tension is related to the phenomenon where matter acts in such a way as to minimize interfaces between phases.

If the interfacial area is increased by $\mathrm{d}A$, there is then an associated free energy cost characterized by

$$\mathrm{d}F = \sigma \, \mathrm{d}A, \tag{3.1}$$

where F is Helmholtz free energy and σ is called surface tension. If there is a finite amount of matter without special boundary conditions, spherical regions of phase separation tend to form, as this geometry minimizes the ratio of area per volume. One should note that the surface area is an ill-defined concept, for even the squared gradient theory predicts smooth transitions between phases. Thus it becomes apparent that there is no unique way to mathematically position the interface. By using a different choice of interface, the associated tension must also change, unless symmetry dictates otherwise, as is the case for planar systems [6].

We now turn our attention to a curved system, following the treatise laid out by Hill [7]. Consider a conical section of a sphere with a solid angle ω in a vacuum, as in Fig. 3.3. Suppose that there are two phases such that if the system is large enough, radius r_α lies in the bulk phase α and radius $r_\beta > r_\alpha$ in the phase β. Our system of interest lies between these two radii. Far from the interface we have bulk pressures P^α and P^β. The system is in complete equilibrium at a temperature T. We introduce c types of molecules to the system and denote their amounts by $\mathbf{n} = (n_1, \ldots, n_c)$. We can thus write the differential of F as follows

$$\mathrm{d}F = -S \, \mathrm{d}T - P^\alpha \omega r_\alpha^2 \, \mathrm{d}r_\alpha + P^\beta \omega r_\beta^2 \, \mathrm{d}r_\beta + \gamma \, \mathrm{d}\omega + \boldsymbol{\mu} \cdot \mathrm{d}\mathbf{n}, \tag{3.2}$$

where γ is the conjugate variable to ω, i.e. the work related to increasing the solid angle by $\mathrm{d}\omega$. If we fix T, r_α and r_β, we may integrate over the remaining extensive variables:

$$\gamma\omega = F - \boldsymbol{\mu} \cdot \mathbf{n}. \tag{3.3}$$

To define an interfacial area between the phases, we must come up with a scheme to define a radius. Suppose that we take any such scheme, be it setting r to the radius where the density of some n_i vanishes, or something completely different. Having

found r, we set out to define the other variables in terms of it. We find for the change in volume

$$\mathrm{d}V^\alpha = \frac{1}{3}(r^3 - r_\alpha^3)\,\mathrm{d}\omega + \omega(r^2\,\mathrm{d}r - r_\alpha^2\,\mathrm{d}r_\alpha), \tag{3.4}$$

$$\mathrm{d}V^\beta = \frac{1}{3}(r^3 - r_\beta^3)\,\mathrm{d}\omega - \omega(r^2\,\mathrm{d}r - r_\beta^2\,\mathrm{d}r_\beta). \tag{3.5}$$

and for the change in area

$$\mathrm{d}A = r^2\,\mathrm{d}\omega + 2\omega r\,\mathrm{d}r. \tag{3.6}$$

Using the equations above, after some algebra one ends up with

$$\mathrm{d}F = -S\,\mathrm{d}T - P^\alpha\,\mathrm{d}V^\alpha - P^\beta\,\mathrm{d}V^\beta + \sigma\,\mathrm{d}A + C\,\mathrm{d}r + \boldsymbol{\mu}\cdot\mathrm{d}\mathbf{n}, \tag{3.7}$$

where

$$\sigma = (F + P^\alpha V^\alpha + P^\beta V^\beta - \boldsymbol{\mu}\cdot\mathbf{n})/A, \tag{3.8}$$

$$C = \omega r^2(P^\alpha - P^\beta) - 2\omega\sigma r. \tag{3.9}$$

Note that r is not an independent variable and could thus be eliminated. Although we have carried out our analysis for a cone, the same equations result for bubbles, even small ones, i.e. the case $\omega = 4\pi$, $r_\alpha = 0$. The term $C\,\mathrm{d}r$ is due to curvature, and can be generalized to systems other than spherical.

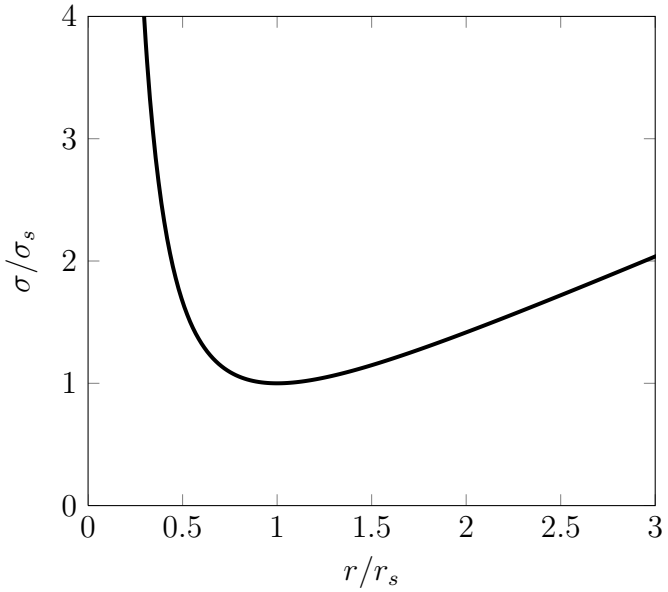

Figure 3.1: The dependence of surface tension on the choice of surface. We denote by r the radius of the chosen surface, r_s the Laplace surface and σ_s the Laplace surface tension.

Suppose now that we vary the condition according to which r is set. This is a purely notional change and thus the total energy of the system must stay unchanged, that is,

$$0 = [\mathrm{d}F] = \sigma[\mathrm{d}A] + C[\mathrm{d}r] - P^{\alpha}[\mathrm{d}V^{\alpha}] - P^{\beta}[\mathrm{d}V^{\beta}], \tag{3.10}$$

where the differentials with square brackets are called formal differentials, as they do not refer to a change in the underlying physical system, but rather to the choice of the definition of surface. Plugging in the spherical shape, we obtain [8]

$$P^{\alpha} - P^{\beta} = \frac{2\sigma}{r} + \left[\frac{\mathrm{d}\sigma}{\mathrm{d}r}\right]. \tag{3.11}$$

This equation is called the Laplace law and the surface where the derivative vanishes is called the surface of tension. Finally, we may solve the differential equation for σ. After some algebra, one finds

$$\sigma = \frac{\int \exp\left(\int \frac{2}{r}\,\mathrm{d}r\right)(P^{\alpha} - P^{\beta})\,\mathrm{d}r + D}{\exp\left(\int \frac{2}{r}\,\mathrm{d}r\right)} = \frac{(P^{\alpha} - P^{\beta})r^3 + 3D}{3r^2}, \tag{3.12}$$

where D is an integration constant to be determined by the boundary condition $\sigma(r_s) = \sigma_s$, where r_s is determined by $\mathrm{d}\sigma/\,\mathrm{d}r\,|_{r=r_s} = 0$. Hence,

$$\sigma = (P^{\alpha} - P^{\beta})\frac{2r^3 + r_s^3}{6r^2}, \tag{3.13}$$

where

$$P^{\alpha} - P^{\beta} = \frac{2\sigma_s}{r_s} \tag{3.14}$$

as expected. We have plotted Eq. (3.13) in Fig. 3.1, from which we can see that the tension is at its minimum at the Laplace surface of tension r_s.

We shall later return to this to give these rather abstract concepts an interpretation based on mechanics.

3.2 Local Pressure

Although the notion of pressure varying within a system is quite old, it is only rather recently that it has been applied to complex biological situations [9]. Most studies have concentrated on lateral pressure profiles of lipid bilayers which can be related to elastic properties of membranes and membrane protein functionality [10–12]. However, some studies have also connected the pressure distribution of spherical particles to the surface tension of the system.

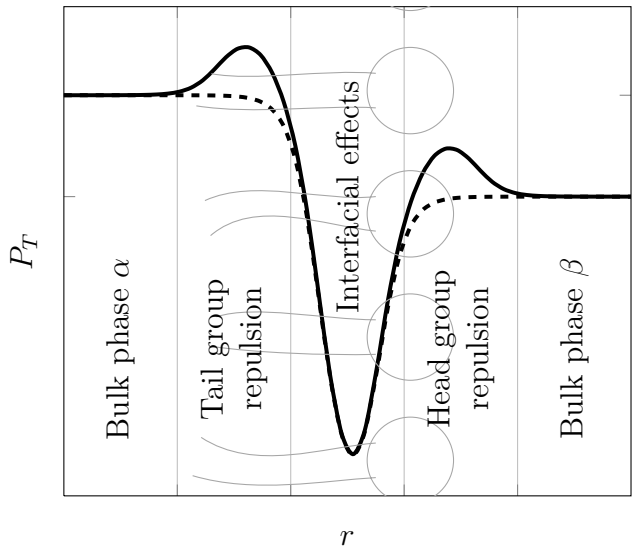

Figure 3.2: A schematic of the tangential pressure profile as a function of distance at an interface of a spherically symmetric lipid system, representing e.g. a unilamellar liposome. The dashed line represents interfacial effects and ignores the microscopic structure, whereas the solid line includes also the effects induced by the surfactant lipids. A sketch of the lipid–water interface is shown in the background

For example, El Bardouni *et al.* [13] calculated local pressure distributions for a spherical droplet of Lennard-Jones fluid in its own vapor. Their result is schematically illustrated by the dashed line in Fig. 3.2. Similar behaviour is predicted also by continuum models [14], which is reasonable since the negative peak corresponds to the effect of surface tension trying to minimize the surface area. However, for lipid droplets having a surface monolayer, more complex phenomena are to be expected based on previous studies of lipid bilayers. There is a repulsion between hydrocarbon tails and head groups arising from steric and entropic interactions, resulting in positive pressure. This effect is illustrated by the solid line in Fig. 3.2. Peaks in these kinds of non-uniform pressure profiles have been found in lipid monolayers and bilayers using several different computational [9] and theoretical methods [15, 16].

From Fig. 3.2 it becomes apparent that the description of surfaces as localized interfaces, as suggested in the previous Section, is not sufficient from a micromechanical point of view.

To describe this idea in a more mathematical way, in the previous Section the system was described by four different quantities, namely the pressures inside and outside the droplet, the surface tension and the associated surface of tension. For large length scales, this parametrization captures the essential properties, but over the scales relevant to this Thesis, the whole profile might be important. One might argue that in these scales one cannot do thermodynamics due to the small number of particles and that even the concept of localized pressure makes little sense [17].

Despite these complications we describe our microscopic droplets using surface tension in an attempt to connect it to macroscopic measurements. We also study its relation to the stability of the particles.

3.3 Surface Tension from Pressure Profiles

In this Chapter we shall derive the connection between local pressure and surface tension, and derive some of their properties. Our treatment follows that of Buff [18]. For a more recent discussion on the subject, see [17, 19]. As our purpose is to describe the elastic properties of lipoparticles, we focus on the case of spherical symmetry. As tensors appearar several times in this Section, we provide a very condensed introduction to the very basics of tensor calculus in Appendix 1. The spherically symmetric pressure tensor in the spherical coordinate system (Fig. A1.1) can be written in a compact form as

$$\mathbf{P}(\mathbf{r}) = P_N(r)\mathbf{e}_r\mathbf{e}_r + P_T(r)(\mathbf{e}_\theta\mathbf{e}_\theta + \mathbf{e}_\varphi\mathbf{e}_\varphi), \tag{3.15}$$

where we have used the dyadic notation, i.e. $\mathbf{e}_r$, $\mathbf{e}_\theta$ and $\mathbf{e}_\varphi$ are the usual basis vectors of the spherical coordinate system (see Appendix 1 for definitions). The functions P_N and P_T represent the normal and the tangential components of the pressure tensor with respect to the spherical interface, respectively.

For brevity and simplicity, we shall opt for a treatise based solely on mechanical grounds and not deal with its connections to the more fundamental approach of thermodynamics, as outlined in Section 3.1. Therefore, in this Section, we consider the concept of surface tension as a model, as a parametric fit to describe the pressure distribution in simpler terms. As such, its meaningfulness at small length scales may be questioned, as explained in Section 3.1.

The approach taken here is to approximate the whole pressure distribution by just four quantities: the two bulk pressures, the surface tension, and the surface of tension. By the surface of tension we mean the surface at which the surface tension acts. This means that the effects caused by the microscopic structure of the surfactant, as discussed in Chapter 3.2, are muddled into the conventional surface effects. Their effect is to lower the surface tension, as can readily be seen from the qualitative picture of Fig. 3.2.

The mechanical surface tension is defined as the difference between the forces exerted by the real and idealized pressure distributions. The surface of the real system has a finite thickness and a characteristic pressure profile. The ideal system is an infinitely thin dividing surface between two bulk phases. To put this on quantitative terms, let us consider a spherically symmetric system depicted in Fig. 3.3. The total

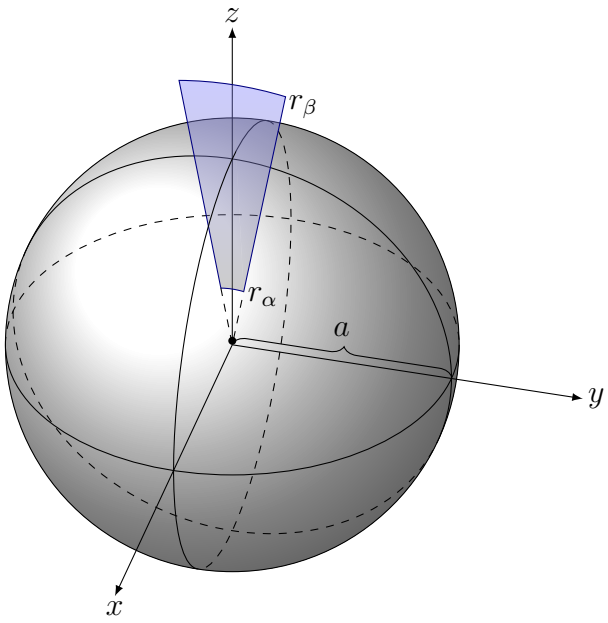

Figure 3.3: An illustration of the concept of surface of tension via an idealized system with a distinct surface on which the surface tension acts

force $\mathrm{d}f$ acting on the angularly infinitesimal sectorial strip $\mathrm{d}\theta$ in the real system is

$$\mathrm{d}f = \mathrm{d}\theta \int_{r_\alpha}^{r_\beta} P_T(r) r \, \mathrm{d}r, \tag{3.16}$$

where r_α and r_β are some radiuses far away from the non-uniform surface and well within the bulk of phases α and β. In the idealized system the pressure distribution has two parts:

1. Bulk pressure $P^{\alpha,\beta}$, which is defined as follows:

$$P^{\alpha,\beta}(r; r_s) = \begin{cases} P^\alpha & \text{, when } r < r_s \\ P^\beta & \text{, when } r > r_s \end{cases}, \tag{3.17}$$

where P^α and P^β are the bulk pressures of phases α and β, respectively, and r_s is the location of the dividing surface, often called the *surface of tension*.

2. Interfacial tension σ, which is localized at the surface of tension r_s and acts in the negative tangential direction, i.e. it tries to minimize the surface area. With the help of the Dirac delta distribution δ, the interfacial tension distribution can be written as

$$\sigma(r; r_s) = -\sigma\delta(r - r_s). \tag{3.18}$$

In the idealized system defined above, the force acting on the strip of Fig. 3.3 would

be

$$\mathrm{d}f = \mathrm{d}\theta \int_{r_\alpha}^{r_\beta} P^{\alpha,\beta}(r; r_s) r \,\mathrm{d}r - \sigma r_s \,\mathrm{d}\theta. \tag{3.19}$$

Setting the expressions (3.16) and (3.19) equal, we arrive at

$$\sigma r_s = \int_{r_\alpha}^{r_\beta} (P^{\alpha,\beta}(r; r_s) - P_T(r)) r \,\mathrm{d}r. \tag{3.20}$$

A similar analysis can be carried out for the torque about the origin, $\mathrm{d}m$. Considering the real system,

$$\mathrm{d}m = \mathrm{d}\theta \int_{r_\alpha}^{r_\beta} P_T(r) r^2 \,\mathrm{d}r. \tag{3.21}$$

For the idealized system,

$$\mathrm{d}m = \mathrm{d}\theta \int_{r_\alpha}^{r_\beta} P^{\alpha,\beta}(r; r_s) r^2 \,\mathrm{d}r - \sigma r_s^2 \,\mathrm{d}\theta. \tag{3.22}$$

Equating the expressions (3.21) and (3.22), one gets the following equation:

$$\sigma r_s^2 = \int_{r_\alpha}^{r_\beta} (P^{\alpha,\beta}(r; r_s) - P_T(r)) r^2 \,\mathrm{d}r, \tag{3.23}$$

and combining Eqs. (3.20) and (3.23):

$$r_s = \frac{\int_{r_\alpha}^{r_\beta} (P^{\alpha,\beta}(r; r_s) - P_T(r)) r^2 \,\mathrm{d}r}{\int_{r_\alpha}^{r_\beta} (P^{\alpha,\beta}(r; r_s) - P_T(r)) r \,\mathrm{d}r}. \tag{3.24}$$

If the system under consideration is in mechanical equilibrium, the divergence of the pressure tensor must vanish, i.e. $\nabla \cdot \mathbf{P} = 0$. This condition in spherical coordinates using the natural coordinate basis can be written as

$$0 = \hat{P}^{ij}_{;i} = \hat{P}^{ij}_{,i} + \Gamma^i_{ki} \hat{P}^{kj} + \Gamma^j_{ki} \hat{P}^{ik}, \tag{3.25}$$

where we have used the Einstein summation convention, Γ^i_{jk} are the Christoffel symbols, and $\hat{P}^{ij}$ are the components of the pressure tensor in the natural coordinate basis. Substituting the Christoffel symbols, we end up with

$$0 = \frac{\partial \hat{P}^{rr}}{\partial r} + \frac{2}{r} \hat{P}^{rr} - r \hat{P}^{\theta\theta} - r \hat{P}^{\varphi\varphi} \sin^2 \theta. \tag{3.26}$$

Thus, by switching back to the physical coordinate basis, we obtain

$$\frac{\mathrm{d}}{\mathrm{d}r}(r^2 P_N(r)) = 2 r P_T(r). \tag{3.27}$$

We proceed by integrating Eq. (3.27):

$$r_\beta^2 P_N(r_\beta) - r_\alpha^2 P_N(r_\alpha) = 2\int_{r_\alpha}^{r_\beta} P_T(r) r \,\mathrm{d}r \tag{3.28}$$

Now using Eqs. (3.17) and (3.20),

$$r_\beta^2 P_N(r_\beta) - r_\alpha^2 P_N(r_\alpha) = 2\left(\int_{r_\alpha}^{r_\beta} P^{\alpha,\beta}(r; r_s) r \,\mathrm{d}r - \sigma r_s\right) \tag{3.29}$$

$$= 2\left(\frac{1}{2}(r_\beta^2 - r_s^2)P^\beta + \frac{1}{2}(r_s^2 - r_\alpha^2)P^\alpha - \sigma r_s\right). \tag{3.30}$$

Finally, we employ the fact that $P_N(r)$ tends to $P^{\alpha,\beta}(r; r_s)$ far from the interface, and choose r_α and r_β accordingly. The natural choice is $r_\alpha \to 0$ and $r_\beta \to \infty$. From these quasi-thermodynamical considerations, we have derived the *Laplace's law*:

$$P^\alpha - P^\beta = \frac{2\sigma}{r_s}. \tag{3.31}$$

One must bear in mind that this equation applies only in the case where r_s is the radius of the surface of tension, i.e. when it is defined by Eq. (3.24). For interfaces of low interfacial tension, the surface of tension is situated far away from the dividing surface. This might be the case in many biological systems [19].

3.4 Continuum Elasticity

In this Section we present some mathematical notations and definitions which somewhat differ from those usually used. These details are important to give the pressure profile program a mathematical basis of some sort.

Suppose a body V undergoes a deformation. We denote a point in the reference configuration by coordinates x^i, the same point in the deformed state by $\bar{x}^i$ and the associated metric by g_{ij}. The relationship between the reference state and the deformed state is given by $\bar{x}^i = x^i + u^i(x)$. Coordinate transformations provide a powerful framework for handling displacements. Therefore, we tackle the problem of describing the deformation in a quite general setting using tensor calculus.

We may write the distance between two adjacent points in the reference configuration as

$$\mathrm{d}s^2 = g_{ij}(x)\,\mathrm{d}x^i\,\mathrm{d}x^j. \tag{3.32}$$

Note that here we use the Einstein summation convention, i.e. we omit sums over repeated indices, see Appendix 1 for details. By the definition of $\mathbf{u}$,

$$\mathrm{d}\bar{x}^i = \mathrm{d}x^i + \mathrm{d}u^i = (\delta^i_k + u^i_{,k})\,\mathrm{d}x^k, \tag{3.33}$$

where δ^i_j is the Kronecker delta and the subscript $,k$ denotes partial differentiation with respect to x^k. We may thus write for the deformed state,

$$\mathrm{d}\bar{s}^2 = g_{ij}(\bar{x})\,\mathrm{d}\bar{x}^i\,\mathrm{d}\bar{x}^j = g_{ij}(\bar{x})(\delta^i_k + u^i_{,k})\,\mathrm{d}x^k(\delta^j_l + u^j_{,l})\,\mathrm{d}x^l, \tag{3.34}$$

which, after some algebra, can be written in the form

$$\mathrm{d}\bar{s}^2 = \left(g_{ij}(\bar{x}) + u_{j,i} + u_{i,j} + g_{kl}(\bar{x})u^k_{,i}u^l_{,j}\right)\mathrm{d}x^i\,\mathrm{d}x^j. \tag{3.35}$$

Denoting the term inside the brackets by $g'_{ij}(x)$, we may write the strain tensor $\varepsilon_{ij}(x)$ by definition as

$$2\varepsilon_{ij}(x)\,\mathrm{d}x^i\,\mathrm{d}x^j = \mathrm{d}s'^2 - \mathrm{d}s^2 = (g'_{ij}(x) - g_{ij}(x))\,\mathrm{d}x^i\,\mathrm{d}x^j. \tag{3.36}$$

As the metric tensor is always symmetrical, so is also the strain tensor.

We illustrate the idea behind $g'_{ij}(x)$ by a simple example. Take a one dimensional situation, with $g_{11}(x) = x^2$ as the metric. This, in simple terms, means that the length of a unit interval at x is $\sqrt{g_{11}(x)} = x$, as by definition $\mathrm{d}s^2 = g_{11}(x)\,\mathrm{d}x^2$. If we move from $x = 0$ to $x = 1$, we move $s = \int_0^1 x\,\mathrm{d}x = 1/2$ units of length. We deform this interval by the mapping $x' = x + (x + 1)$, i.e. $[0, 1] \to [1, 3]$. The length of the new interval may be computed as $s' = \int_1^3 x'\,\mathrm{d}x' = 4$, so the deformation is an elongation. We however pursue a different route. The idea of the preceding discussion may be summed up as trying to transform the integral over the deformed state (the interval $[1, 3]$) into an integral over the reference state (the interval $[0, 1]$), i.e. $4 = s' = \int_0^1 \sqrt{g'_{11}(x)}\,\mathrm{d}x$, with $g'_{11}(x)$ to be determined. In this simple example, one immediately sees, by using the standard integration by substitution, that $g'(x) = 4 \cdot (2x + 1)^2$, which indeed coincides with Eq. (3.35).

It has been gradually realized that the traditional continuum mechanical definitions of stress as the tensor whose divergence equals force, do not generalize directly to microscopic scales [20–24]. Therefore, instead of defining a stress independently of strain, we define it as a conjugate variable of sorts to the strain tensor. We define the stress tensor σ^{ij} so as to satisfy the following equation

$$\delta F = \int_V \sigma^{ij}\delta\varepsilon_{ij}\sqrt{g}\,\mathrm{d}x, \tag{3.37}$$

where δF is a variation to the free energy and g is the determinant of the metric tensor. In other words, the stress tensor may be expressed as a functional derivative [25]

$$\sigma^{ij} = \frac{1}{\sqrt{g}}\frac{\delta F}{\delta\varepsilon_{ij}}. \tag{3.38}$$

As the free energy is usually difficult to obtain in terms of the strain tensor, we use Eq. (3.36) and the properties of functional derivatives to transform the problem of decribing deformations into one describing changes in coordinates [20],

$$\frac{1}{2}\sqrt{g}\,\sigma^{ij} = \frac{\delta F}{\delta g_{ij}}, \tag{3.39}$$

or in an equivalent form

$$-\frac{1}{2}\sqrt{g}\,\sigma_{ij} = \frac{\delta F}{\delta g^{ij}}. \tag{3.40}$$

Note that since the strain tensor is symmetric, so is the stress tensor.

For convenience, we define a quantity called the pressure tensor simply as the negative of the stress tensor, i.e.

$$P^{ij} = -\sigma^{ij}. \tag{3.41}$$

That the divergence of the stress tensor vanishes,

$$\sigma^{ij}_{;i} = 0, \tag{3.42}$$

follows from the translation invariance of the free energy, which in turn is a consequence of Liouville's theorem [21]. At least qualitatively the result of Eq. (3.42) is clear, for the divergence of the stress tensor represents the force acting on a material point. Such forces must vanish if the system is to be in equilibrium.

3.5 Helfrich Elasticity

Helfrich [26] derived the now well established mathematical model for lipid bilayer elasticity. The model has subsequently been generalized to a broad class of problems [19]. In the following, we give a simple justification to the Helfrich form of curvature energy, as per Safran [6], by deriving the equations from a microscopic toy model. In all generality Helfrich theory is essentially just a Taylor expansion in curvature, but the resulting formulas of the following treatment provide clear interpretation for the Taylor expansion constants.

We consider a spherical structure of n lipids, such as the one depicted in Fig. 3.4. Modelling each lipid as an ideal spring obeying the usual Hooke's law, we can write the energy per lipid as

$$f = \frac{1}{2}k_s(\ell - \ell_s)^2, \tag{3.43}$$

where k_s is the spring constant, ℓ the length of the spring, representing the length of

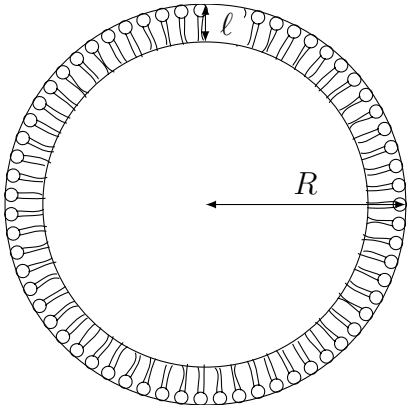

Figure 3.4: Toy model of a spherical lipid assembly.

the lipid tail projected to the normal of the bilayer and ℓ_s the equilibrium length of the spring. We further assume incompressibility, i.e. if the springs as a whole are compressed, the size of the complex increases so as to keep the volume per lipid constant. This type of behaviour is typical of rubber and an assumption often used in self-consistent polymer field theory [27].

Calculating the volume per lipid under the assumption that the radius of the system is larger than the length of the lipids, i.e. $\ell < R$,

$$v_0 = \frac{4}{3}\pi(R^3 - (R-\ell)^3)/n = \frac{4}{3}\pi\ell(\ell^2 - 3\ell R + 3R^2)/n \tag{3.44}$$

$$= A_0\ell\left(1 - H\ell + \frac{1}{3}K\ell^2\right), \tag{3.45}$$

where A_0 is the area per lipid, $H = 1/R$ the mean curvature, and $K = 1/R^2$ the Gaussian curvature. The two curvature terms, H and K, are independent when considering more general surfaces. As we restrict our discussion to the spherical case, we shall henceforth use H^2 in place of K.

Assuming $\ell H \ll 1$, i.e. the thickness of the lipid surface is negligible compared to the radius of the system, we can employ regular perturbation theory [28] to solve Eq. (3.45) for ℓ. Up to second order in H

$$\ell = \ell_0 + \ell_0^2 H + \frac{5}{3}\ell_0^3 H^2 + \mathcal{O}(\mathcal{H}^\ni), \tag{3.46}$$

where $\ell_0 = v_0/A_0$.

Substituting this back to Eq. (3.43), and once again ignoring terms of order $\mathcal{O}(\mathcal{H}^\ni)$, we arrive at the approximate formula first derived by Helfrich [26]:

$$f = 2k(H - c_0)^2 + \bar{k}K, \tag{3.47}$$

where k is called the bending modulus, c_0 the spontaneous curvature, and $\bar{k}$ the

Gaussian bending (or saddle-splay) modulus. They are given by the expressions [29]:

$$c_0 = \frac{\ell_s - \ell_0}{\ell_0^2}, \qquad k = \frac{1}{4} k_s \ell_0^4, \qquad \bar{k} = -\frac{5 c_0 k_s \ell_0^5}{3}. \tag{3.48}$$

From the expression for c_0 we see that if the area per lipid, A_0, decreases while keeping the volume, v_0, constant, ℓ_0 increases resulting in a negative spontaneous curvature. The opposite is true if we increase A_0. We therefore deduce that the spontaneous curvature describes the ratio of the size of the head group and that of the tail group. The sign convention is sketched in Fig. 3.5.

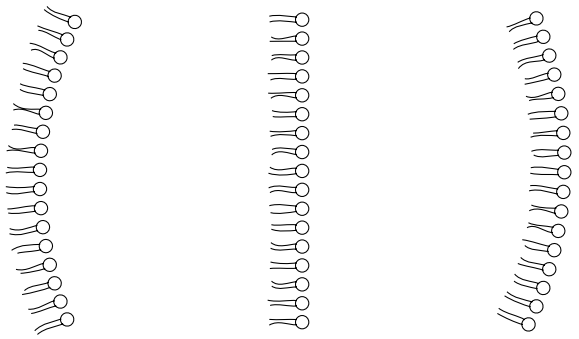

Figure 3.5: Lipid membranes with negative, zero and positive spontaneous curvatures, respectively.

For a spherical surface we minimize the free energy, i.e. Eq. (3.47) multiplied by the area $4\pi R^2$, and obtain

$$R_{\text{eq}} = \frac{1}{c_0}. \tag{3.49}$$

This has to, in order to be stable, fulfill the condition $\partial^2 f / \partial R_{\text{eq}}^2 > 0$, i.e. $k > 0$.

It is worth pointing out that Eq. (3.47), with K placed appropriately, applies to membranes of arbitrary shape, assuming that their curvature is modest. Furthermore, upon integrating Eq. (3.47) over a closed surface, the rightmost term effectively vanishes. This is due to a fundamental differential geometric relation called the Gauss–Bonnet theorem, which states that a closed surface integral of K equals a topological constant [6]. Therefore the value of $\bar{k}$ is hardly of interest in static situations, but it might play a role in lipoprotein fusion where the topology undergoes changes.

It is of some concern that the lipoproteins analyzed in this study are approximately 10 nm in diameter while the surfactant monolayer at the surface of the lipoprotein particle is some 2 nm in thickness. This situation of high curvature means that the approximations made by the Helfrich theory of elasticity do not apply very well. We shall, however, stick to this established theory as a reasonably good approximation.

It is difficult to deduce the parameters, such as ℓ_s, of the model outlined above. We therefore develop the notion of pressure profile, a simple but instructive model, which relates the constants k, $\bar{k}$ and c_0 to more molecular properties.

3.5.1 Curvature Dependence of Interfacial Tension

Having introduced the theory of Helfrich, in this short Section we shall generalize Laplace's law (Eq. (3.31)) and connect it to the Helfrich constants. This is done by combining the treatments of Blokhuis & Bedeaux [30] and Rowlinson & Widom [17]. We start by defining the surface tension of a more general surface, characterized by a radius R, which need not be the radius of the surface of tension. We define, following the form of Eq. (3.23),

$$\sigma(R) = \int_{r_\alpha}^{r_\beta} (P^{\alpha,\beta}(r;R) - P_T(r)) \left(\frac{r}{R}\right)^2 \mathrm{d}r. \tag{3.50}$$

We proceed by calculating the derivative of $\sigma(R)$:

$$\frac{\mathrm{d}\sigma(R)}{\mathrm{d}R} = \int_{r_\alpha}^{r_\beta} \frac{\mathrm{d}}{\mathrm{d}R} \left((P^{\alpha,\beta}(r;R) - P_T(r)) \left(\frac{r}{R}\right)^2 \right) \mathrm{d}r \tag{3.51}$$

$$= \int_{r_\alpha}^{r_\beta} (P^\alpha - P^\beta)\delta(R-r) \left(\frac{r}{R}\right)^2 + (P^{\alpha,\beta}(r;R) - P_T(r)) \left(-\frac{2r^2}{R^3}\right) \mathrm{d}r \tag{3.52}$$

$$= P^\alpha - P^\beta - \frac{2\sigma(R)}{R}, \tag{3.53}$$

where we have employed the fact that the derivative of the Heaviside function is the Dirac delta distribution. By rearranging, we arrive at

$$P^\alpha - P^\beta = \frac{2\sigma(R)}{R} + \frac{\mathrm{d}\sigma(R)}{\mathrm{d}R}. \tag{3.54}$$

We used Eq. (3.23) as the point of departure as it is more fundamental than the alternative forms in the sense that it relates directly to the work associated with a displacement of the surface (see Refs. [17, 19] for a more thorough justification).

From the discussion in Section 3.5, we conclude that

$$\sigma = f_0 + 2k(H - c_0)^2 + \bar{k}K, \tag{3.55}$$

where $f_0 + 2kc_0^2 = \sigma_0$, the surface tension of a planar interface and $H = 1/R$, $K = 1/R^2$, as before. Employing Eq. (3.54), Laplace's law may be written in the form

$$P^\alpha - P^\beta = \frac{2\sigma_0}{R} - \frac{2kc_0}{R^2}. \tag{3.56}$$

This is to be contrasted with the definition of Tolman length [31]. Notice that as we have taken the Helfrich energy into application, we have fixed R as a physical radius of the droplet, or more precisely the neutral surface of bending. We have thus shown that the curvature dependence of the mechanical surface tension can be approximated by using elastic curvature energy of the surface.

4. MODELLING LIPOPROTEIN FUSION

Although lipid bilayer and vesicle fusion have been widely studied (see e.g. Ref. [32] and references therein), there are only a few studies on lipid droplet fusion. In this work, we relate lipid droplet fusion to the initial stages of vesicle fusion.

The best known model for lipid bilayer fusion is the so called stalk model introduced by Markin *et al.* [3]. The first stage of this fusion mechanism is the formation of a neck-like connection between the outer leaflets, generating a metastable state called hemifusion, as shown is Fig. 4.1. Should the inner leaflets also connect, full fusion would follow. Using the original stalk model, it was demonstrated that the stalk formation energy decreases with decreasing spontaneous curvature.

However, in more recent studies, triggered by Katsov *et al.* [33] using self-consistent field theory and Monte Carlo simulations, it was shown that the picture of Markin *et al.* [3] is overly simplistic and does not capture the mechanism beyond the initial steps, and also that the stalk energy dependence on spontaneous curvature is not obvious. What these later studies do agree on is that the stalk formation is an important intermediate step towards bilayer fusion. Only these initial steps of bilayer fusion are relevant to lipoparticle fusion, as lipoparticles consist of a monolayer rather than a bilayer. Below, we review the original model of Markin *et al.* [3] and show that one might expect the spontaneous curvature to have an effect on the stalk formation energy, and thus the fusion rate. We also discuss more recent developments of fusion models based on the Helfrich theory.

The stalk formation is not necessarily the rate limiting step of fusion. Instead, it has been suggested that the fusion process starts when one hydrocarbon tail flops into the monolayer of the other particle [34] (Fig. 4.2). This results in a situation with one phospholipid hacing a tail in both particles. The site finally grows to stalk. This process has been seen in molecular level simulations [35]. Negative spontaneous curvature would facilitiate tail flopping by making the hydrocarbon tails more packed. Thus, spontaneous curvature enters into discussion about fusion through two distinct processes, namely stalk formation energy and tail flopping energy.

4.1 Mathematical Model of Stalk Formation

The stalk model for bilayers, as it is most often applied to, can be easily explained in qualitative terms. We assume that the mechanism of fusion has to be more or

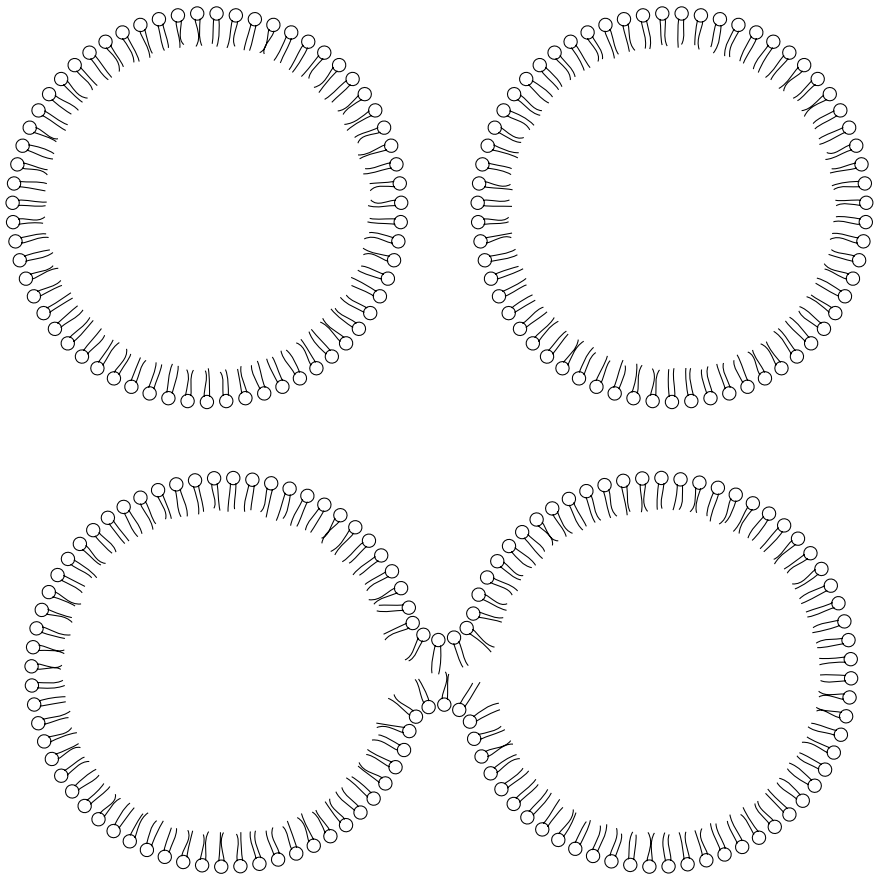

Figure 4.1: A schematic representation of the stalk theory of fusion applied to lipoparticles.

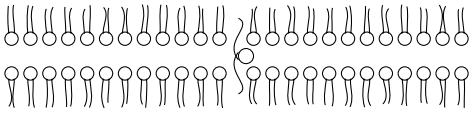

Figure 4.2: A schematic representation of the initial step of fusion as suggested by Kinnunen [34].

less like the one depicted in Fig. 4.1. For lipid droplets it is reasonable to assume that the stalk formation energy is directly related to the fusion barrier. This is not the end of the process for bilayer structures such as vesicles, however, for they still have the inner leaflet to fuse. This kind of metastable state, called hemifusion, is very difficult to analyze as several fusion mechanisms for the inner leaflets have been suggested. Fortunately, this is of little consequence to this Thesis, since we shall only be concerned with monolayer structures.

A mathematical treatise of the stalk model was first carried out by Markin *et al.* [3]. Although qualitatively it yielded reasonable results, a more quantitative look revealed serious shortcomings, as the model overestimated the stalk formation energy. The overestimation is so large that according to the theory, fusion should never happen in practice. This flaw has subsequently been straightened out by relaxing the

assumptions on the shape of the stalk and by generalizing the Helfrich elastic energy (Eq. (3.47)) to take lipid tilt into account [36–38]. In this work, we shall review in detail only the simple original version of the model so as to justify why the stalk formation energy might depend on spontaneous curvature.

4.1.1 The Original Theory of Markin *et al.*

We start by writing out Eq. (3.47) in terms of the two principal curvatures (c_r, c_h) and drop the term related to Gaussian bending, assuming that it is small:

$$f = \frac{k}{2}(c_r + c_h - 2c_0)^2. \tag{4.1}$$

As we can see from Fig. 4.1, the formed stalk is approximately the inner loop of a torus, as illustrated in Fig. 4.3.

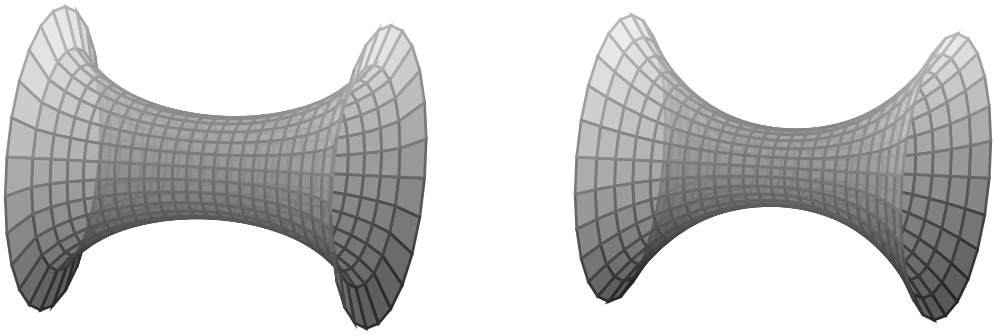

Figure 4.3: The two stalk shapes discussed in this Thesis: the inside of a torus and a catenoid, respectively

Carrying on with the mathematical treatment, from Fig. 4.4 one immediately sees that $h = a + r - \sqrt{r^2 - x^2}$, $n_y = \sqrt{r^2 - x^2}/r$. Furthermore, $(h')^2 = x^2/(r^2 - x^2)$. The curvatures given in terms of these quantities are therefore (see Appendix 1 for the definition of curvature)

$$c_r = -\frac{1}{r} \tag{4.2}$$

$$c_h = \frac{n_y}{h} = \frac{\sqrt{r^2 - x^2}/r}{a + r - \sqrt{r^2 - x^2}}. \tag{4.3}$$

When the stalk is formed, the change in elastic energy is

$$W_s = \frac{k}{2}\left(\int_{\text{stalk}} (c_r + c_h - 2c_0)^2 \,\mathrm{d}A - \int_{\text{stalk}} (2c_{\text{init}} - 2c_0)^2 \,\mathrm{d}A\right), \tag{4.4}$$

where the last term on the right is simply the area of the stalk times the curvature

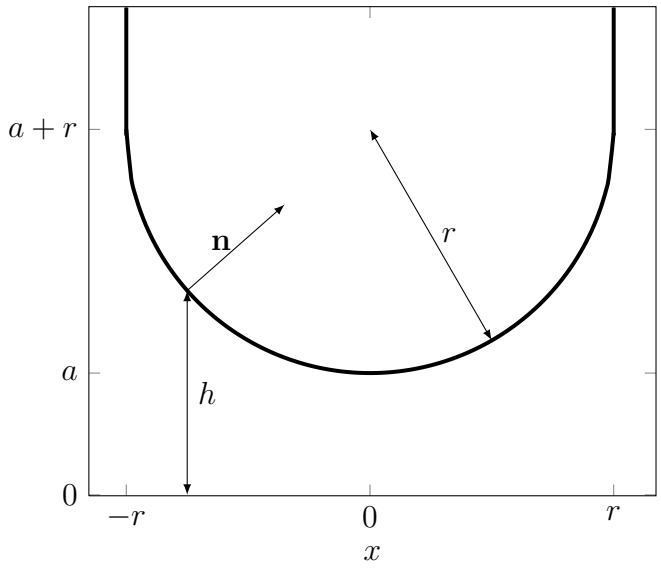

Figure 4.4: The stalk approximated as the inner part of a torus (toroidal stalk)

energy per unit area of the situation before stalk formation. We evaluate the first term on the right hand side of Eq. (4.4):

$$W_f = \frac{k}{2} \cdot 2\pi \int_{-r}^{r} (c_r + c_h - 2c_0)^2 \, h\sqrt{1 + (h')^2} \, \mathrm{d}x. \tag{4.5}$$

Carrying on with the integration, and computing the latter part of Eq. (4.4) in a similar manner, we arrive at

$$\begin{aligned} W_s = 4\pi k \Bigg(& \left(\left(\frac{1}{r} + c_0 \right)^2 - (c_{\mathrm{init}} - c_0)^2 \right) \left(\pi r(r+a) - 2r^2 \right) \\ & -\pi \left(\frac{1}{r} + c_0 \right) (r+a) + \frac{(r+a)^2}{r\sqrt{a(2r+a)}} \arctan \sqrt{\frac{2r+a}{a}} \Bigg). \end{aligned} \tag{4.6}$$

For illustrative purposes, we fix $c_{\mathrm{init}} = 0\,\mathrm{nm}^{-1}$, $a = 1\,\mathrm{nm}$ and minimize W_s with respect to r, while varying c_0. The result is shown in Fig. 4.5. We notice that the stalk formation energy becomes lower with decreasing spontaneous curvature.

4.1.2 Recent Developements

Although the stalk theory of fusion initially showed great prospect, it was soon discovered to be handicapped by what Kozlovsky & Kozlov [37] called the Energy Crisis: The energies predicted by the theory were far too great to match experimental results.

Several authors have now reconciled this discrepancy by relaxing the assumption made on the shape of the stalk [36–38]. As we have seen in the previous Section,

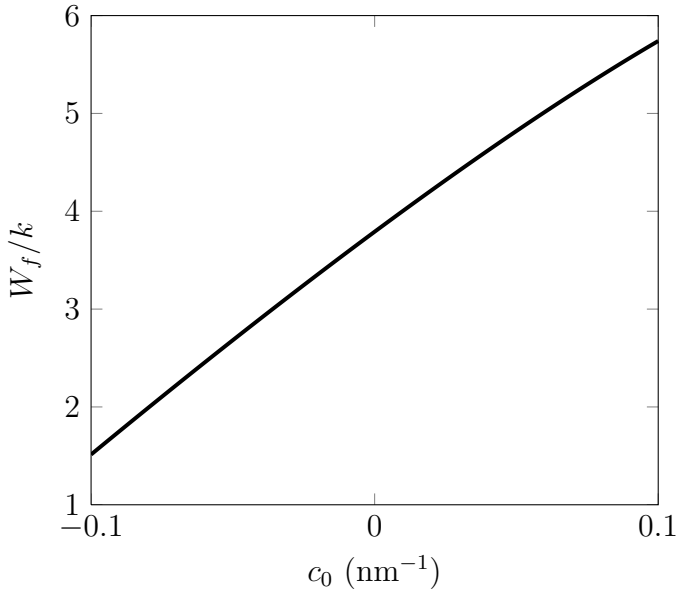

Figure 4.5: The energy of stalk formation as a function of spontaneous curvature, as predicted by the original model of Markin *et al.*

the original stalk model assumed a toroidal stalk, which turns out not to be of the optimal shape. This is most evident when we consider an axisymmetrical surface with zero mean curvature, called the catenoid (Fig. 4.3). Should the stalk be of infinite size, it could take this shape, and when $c_0 = 0$, no energy would go into its formation. However, no toroidal shape has nonvanishing mean curvature, and therefore always requires energy to form. As physical processes tend to minimize their free energies, the stalk will most likely not be of toroidal shape.

Another assumption made by the original theory should be questioned, namely that of vanishing Gaussian bending. This assumption was born out of necessity, as in the 80s, very little was known about the magnitude of the Gaussian bending modulus. Modern theories should, however, allow for nonvanishing Gaussian bending as discussed by Siegel [39]. Taking this into account, the fusion energies once again become rather high. However, as hinted earlier, this energy does not depend on the stalk shape, courtesy of the Gauss–Bonnet theorem.

Yet another point of worry is that the theory of stalk fusion is built upon Helfrich bending energy, which in turn is based on a Taylor expansion to the second degree in curvature. Not only are the curvatures of lipoprotein droplets high, the stalk curvatures are exceedingly high. However, Markin & Albanesi [36] argued that the Helfrich theory is so well established in a variety of situations that it is reasonable to expect it to provide results of sufficient accuracy even in extreme conditions.

Some modern theories suggest nonsmooth stalk shapes so as to eliminate the voids, or interstices, in bilayer fusion (see Fig. 4.6). They take into account the energy arising from these non-smooth deformations by using the so-called lipid tilt modulus [26, 37, 38]. May [38] even takes into account the change of shape of the

inner monolayer. However, the author of this Thesis believe that in lipoprotein fusion, these voids will be filled by the hydrophobic core instead of surfactant lipid tails. Therefore, we feel that it is unnecessary to consider lipid tilt.

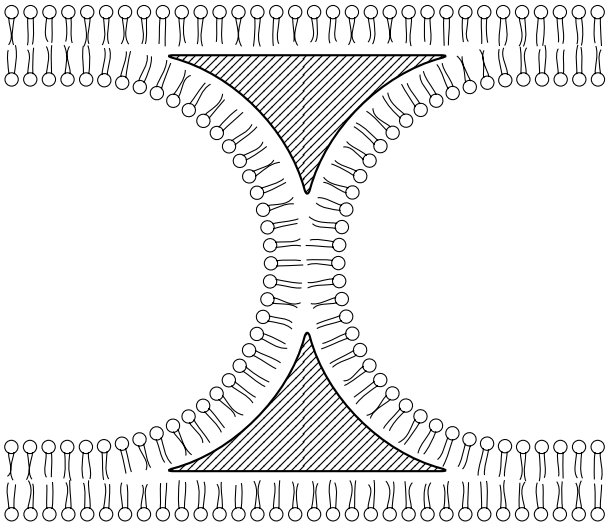

Figure 4.6: A schematic representation of the voids in bilayer stalk formation.

Another model based on the Helfrich functional form is that by Kabalnov & Wennerstrom [40]. This theory is aimed at explaining fusion in emulsions, and at a quick glance is quite applicable to the situation of this Thesis. However, this model implicitly assumes excess lipids in the solvent, which would indeed be the case in emulsions where the critical micelle concentration is exceeded, but is not applicable to the present study. This model is the basis for the study by Rekvig & Frenkel [4]. This computational study, employing dissipative particle dynamics and other novel methods, has many insights into the problem of fusing emulsions. However, the computational model developed in Ref. [4] suffers from one severe issue. The configuration with no surfactants, and thus with the highest surface tension, ought to fuse almost instantaneously, but in the study mentioned above, fusion is not visibly accelerated, but is actually slower.

The study by Rekvig & Frenkel [4] is well-motivated, since stalks indeed are not quite within the approximations made in the Helfrich theory and more microscopic studies are needed to study the applicability of the theory. There is an interesting development made by using self-consistent field theory (SCFT) to study the fusion process [33]. While not quite as microscopic as atomistic molecular dynamics (MD) simulations, SCFT is able to capture more details than a continuum theory and values for different quantities are much easier to extract from SCFT than from a MD simulation.

In general, most of the experimental and theoretical studies support the idea that negative spontaneous curvature should facilitate stalk formation and thus lipid

droplet fusion. The reason, however, is unknown. Furthermore, it is unclear whether these results hold for very small droplets, such as HDL and LDL. In droplets of this kind, surface tension can diverge from the macroscale value and might interfere with the fusion process. One of the objectives of this Thesis is to better understand these effects.

5. METHODS

5.1 Molecular Dynamics

For systems consisting of thousands of molecules and whose analysis requires atomic scale accuracy, Molecular Dynamics (MD) is often the simulation method of choice [41]. Modelling chemical reactions requires the tools of quantum mechanics, which can be coupled with MD through the Car–Parrinello method [42]. However, in this study we model the physics of soft matter, i.e. strong chemical bonds are not broken or formed in the time scales of interest, and therefore chemical reactions in terms of bond breaking can be neglected altogether [25]. This is of course an approximation as especially reactions involving single protons do in fact occur in experiments, but unfortunately they cannot be taken into account in simulations without a severe increase in the computational load.

MD is based on integrating the classical Newton's equations of motion

$$m_i \frac{\mathrm{d}^2 \mathbf{r}_i}{\mathrm{d}t^2} = -\nabla_{\mathbf{r}_i} \Phi(\{\mathbf{r}_j\}). \tag{5.1}$$

Although this is a differential equation, the most commonly used integration algorithms, such as the Runge–Kutta method, are typically not employed due to their non-symplecticity, which would make them prone to drifts in the system energy, one of the key quantities when doing numerical statistical mechanics. For MD simulations, the velocity Verlet and the leap-frog algorithm are the two most common integration algorithms. Both have the advantage of being time-reversible and symplectic [43]. GROMACS 4.0 [44], the MD software used in this study, uses the latter, which we summarize as follows

$$\mathbf{v}_i \left(t + \frac{\Delta t}{2} \right) = \mathbf{v}_i \left(t - \frac{\Delta t}{2} \right) + \frac{\mathbf{F}_i(t)}{m_i} \Delta t \tag{5.2}$$

$$\mathbf{r}_i \left(t + \Delta t \right) = \mathbf{r}_i(t) + \mathbf{v}_i \left(t + \frac{\Delta t}{2} \right) \Delta t. \tag{5.3}$$

We shall not go into the technical implementation in any more detail, as itcan be readily found in a number of other sources [43–45].

5.1.1 MARTINI Force Field

Force field is a parametrization of forces. It contains both the functional forms and the parameters of interactions. MD simulations typically employ two-body, three-body and four-body potentials, and in the following we shall describe these interactions a bit more precisely.

While our discussion here is rather general, we focus on one particular model that is central to this work: the so-called MARTINI force field [46, 47]. It has been designed to model molecular systems comprised of e.g. lipids, proteins, and carbohydrates in a coarse-grained manner. Therefore it is rather optimal for our purposes.

The types of forces used in MD simulations can be split into two categories, namely bonded and non-bonded interactions. The former represents strong bonds, which cannot be broken or formed, and are typically of short range, while the latter are of long range and are usually of the strength of thermal fluctuations.

Let us first consider non-bonded interactions. Two freely rotating dipoles have an average attractive interaction energy proportional to r^{-6}, where r is the interparticle distance [48]. It is quite reassuring to notice that this behaviour is predicted even by the quantum mechanical Drude model [45]. This attractive interaction is sometimes called the Keesom force and it can be regarded as the source of the dispersive van der Waals interaction. This is, however, temperature dependent, which makes all the following parametrizations invalid when the temperature is changed. The effect of the described forces is appropriately accounted for in the much used Lennard-Jones potential:

$$U_{LJ}(\mathbf{r}_i, \mathbf{r}_j) = \frac{C_{ij}^{(12)}}{r_{ij}^{12}} - \frac{C_{ij}^{(6)}}{r_{ij}^{6}}, \tag{5.4}$$

where the r^{-12} term is due to steric, repulsive interactions, whose true origin is the Pauli exclusion principle. The potential given by Eq. (5.4) is approximate, but it is in reasonable agreement with quantum mechanical calculations and experimental results. Although probably the most used, the Lennard-Jones potential is not the only nor the most accurate form devised for the interaction [44].

Two charged particles interact through the Coulombic potential,

$$U_C(\mathbf{r}_i, \mathbf{r}_j) = \frac{k q_1 q_2}{r_{ij}}, \tag{5.5}$$

where q_i are the charges of the particles.

Mocing on, the most typical bonded interaction is the covalent bond which is

described in MARTINI by the harmonic potential,

$$U_H(\mathbf{r}_i, \mathbf{r}_j) = \frac{1}{2}k(r_{ij} - r_{\text{eq}})^2, \tag{5.6}$$

where r_{eq} is the equilibrium distance. Harmonic potential of the cosine type is used to represent chain stiffness

$$U_A(\mathbf{r}_i, \mathbf{r}_j, \mathbf{r}_k) = \frac{1}{2}k(\cos\theta_{ijk} - \cos\theta_{\text{eq}})^2. \tag{5.7}$$

Finally, to prevent out-of-plane distortions, we have the improper dihedrals

$$U_I(\mathbf{r}_i, \mathbf{r}_j, \mathbf{r}_k, \mathbf{r}_l) = \frac{1}{2}k(\theta_{ijkl} - \theta_{\text{eq}})^2. \tag{5.8}$$

In this study we use essentially the same force field parameters as in [49], which are based on a pre-release of the MARTINI force field [47]. However, the superrepulsive interactions between tail ends and polar residues were changed to repulsive since the superresulsive interactions were causing unrealistically stable monolayers. The original MARTINI model [46], on the other hand, is not suitable due to overestimation of spontaneous curvature [50].

5.1.2 Biasing Potential

Since spontaneous fusion is a very rare event in the timescales accessible to modern MD simulations, we introduce an attractive potential between the two particles which we expect to fuse. By altering the strength of this interaction, we can greatly enchance the fusion rate, but the more we steer the simulation, the more the free energy landscape is altered and artifacts are introduced in the form of unphysical fusion paths/processes. As even a small bias will cause some errors in the fusion rates, if not the process itself, the results of this study should be considered on a more qualitative level, as opposed to quantitative. Even so, we expect that the relative fusion rates are not greatly disturbed and that we can draw conclusions for relative stability between different lipid compositions.

The biasing potential used in this Thesis is of the form of harmonic interaction. This form was selected partly because it is already a part of the GROMACS package and is thus robust and convenient to use. Another justification for this type of potential is that fusion events can be quantitatively located in time, defining the zero force as the point where fusion occurs.

The harmonic potential is not ideal, for in principle it distorts the free energy landscape. The optimal biasing potential is a linear one, which can be reasonably approximated by the harmonic one when the interaction constant is small enough as

is the case in our simulations.

The potential pulled together the core molecules of each particle, rather than the whole particles. The equilibrium distance for the centers of masses of the pulled particles was 7 nm and the harmonic constant used in this work 25 kJ mol^{-1} nm^{-1}. The values were determined by experimentation to make the fusion times of the order of 100 ns and were subsequently held fixed in all cases.

5.2 Pressure Profiles from MD Simulations

In previous Chapters the concept of local pressure and its connection to surface tension was introduced. In the following, a way to calculate the local pressure from statistical mechanical quantities is derived. This leads to an expression computable from MD simulations, which further leads to a way to compute surface tension. We follow closely the treatment of Mistura [21], who derives a uniquely defined pressure tensor by differentiating the free energy with respect to the metric tensor. This treatment is not the only one that has been suggested, but it serves its purpose here to provide at least solid qualitative insight.

Because the problem related to defining the pressure tensor still remains debated, the derivation that follows is not widely known. Rather, the paper by Schofield & Henderson [22] is often cited. In the latter, the pressure tensor is defined as a quantity whose derivative is the force, immediately suggesting possible problems with gauge fixing. This method indeed produces a nonunique pressure tensor, which in turn poses several difficult problems when actual physical quantities are calculated from it. This is especially true when the underlining geometry is curved [17]. One should note that from physical considerations the gauge cannot be arbitrarily fixed, for the pressure tensor is supposed to coincide with the well defined homogeneous pressure in the homogeneous limit [51]. This is not taken into account in the derivation presented in [22], and thus has spawned a multitude of papers trying to reach a unique pressure tensor by adding further physical constraints [52].

The pressure tensor presented in [22] coincides with the one in [21] if one chooses Irving–Kirkwood (IK) as the integration contour [53]. The idea of the present derivation is also quite similar to that of Refs. [24, 54]. It is a well known fact that an alternative integration contour called Harasima (H) [55] is physically wrong in many situations, especially when the geometry is not flat [30, 56].

In the following we shall be employing the calculus of variations, and within this framework it is easy to explain why one might obtain a nonunique tensor. This happens for example if one constraints the geometry to a flat manifold before the variational procedure [57], which eliminates some variational modes and results in incorrect equations.

The mathematics of the Helfrich theory was originally in a similar state of crisis,

for several nonequivalent shape equations could be derived. It was later realized that this discrepancy was due to incorrectly fixing the geometry to e.g. an axisymmetrical one before doing the variational mathematics [58, 59]. Indeed as accounted in Ref. [17], the nonuniqueness is said to stem from the fact that inhomogeneous fluids can be deformed in different ways, giving way to different integration contours. This argumentation, as the author of the present Thesis thinks, closely resembles that of the variational calculus arguments given before.

A novel treatment, similar to the one by Mistura, but even more rigorous on the part of statistical thermodynamics, has been recently published [60, 61]. They claim a simpler, but more importantly a unique, form for the pressure tensor when the interactions are of short length. This they extend to long range interactions and recover the usual IK form. However, they claim that smoothness properties required for thermodynamics are not automatically satisfied by this form.

5.2.1 Definition and Contour Independence

Assuming there's no external field, the Hamiltonian of an N-particle system may be written as

$$\mathcal{H} = \sum_{n=1}^{N} \frac{\mathbf{p}_n^2}{2m_n} + \Phi(\mathbf{r}_1, \ldots, \mathbf{r}_N), \tag{5.9}$$

where $\mathbf{p}_n$, m_n are the momenta and masses of each particle, respectively and Φ is the interparticle potential. The kinetic energy may then be written simply as

$$\mathcal{K} = \frac{1}{2} \sum_{n=1}^{N} m_n g_{ij}(x_n) \dot{x}_n^i \dot{x}_n^j. \tag{5.10}$$

As we recall from Hamiltonian mechanics, the conjugate momenta are defined as

$$y_{ni} = \frac{\partial \mathcal{K}}{\partial \dot{x}_n^i} = m_n g_{ij}(x_n) \dot{x}_n^j = m_n \dot{x}_{ni}, \tag{5.11}$$

and thus

$$\mathcal{K} = \frac{1}{2} \sum_{n=1}^{N} \frac{1}{m_n} g^{ij}(x_n) \dot{y}_{ni} \dot{y}_{nj} = \frac{1}{2} \int \rho(x) g^{ij}(x) \dot{y}_{ni} \dot{y}_{nj} \, \mathrm{d}x, \tag{5.12}$$

where we have introduced the density-like quantity,

$$\rho(x) = \sum_{n=1}^{N} \frac{1}{m_n} \delta(x - x_n). \tag{5.13}$$

Given the distances between all the atoms, one may recover their positions (up to

rotations, translations and reflections) by for example multidimensional scaling [62]. Thus the interparticle potential may be written as a function of distances between the particles. The distance between particles x_a and x_b may be expressed as follows.

$$r_{ab} = \int_0^1 \sqrt{g_{ij}(\lambda)\frac{\mathrm{d}x^i}{\mathrm{d}\lambda}\frac{\mathrm{d}x^j}{\mathrm{d}\lambda}}\,\mathrm{d}\lambda, \tag{5.14}$$

where $x^i = x^i(\lambda)$ is the parametric equation of a straight oriented line joining the particles in question and

$$g_{ij}(\lambda) = \int \delta(r - x(\lambda))g_{ij}(r)\,\mathrm{d}r. \tag{5.15}$$

By the definition of the canonical partition function Z and its dependence on the Helmholtz free energy (Eq. 3.40), we may write the pressure tensor $p_{ij}(x)$ as

$$\frac{1}{2}\sqrt{g}p_{ij}(x) = \frac{\delta F}{\delta g^{ij}(x)} = -k_B T\frac{1}{Z}\frac{\delta Z}{\delta g^{ij}(x)} = \left\langle \frac{\delta \mathcal{H}}{\delta g^{ij}(x)} \right\rangle. \tag{5.16}$$

We thus calculate the kinetic contribution,

$$\frac{\delta \mathcal{K}}{\delta g^{ij}(x)} = \frac{1}{2}\rho(x)y_{ni}y_{nj}, \tag{5.17}$$

and the configurational contribution separately,

$$\frac{\delta \Phi}{\delta g_{ij}(x)} = \sum_{a=1}^{N-1}\sum_{b=a+1}^{N}\frac{\partial \Phi}{\partial r_{ab}}\frac{\delta r_{ab}}{\delta g_{ij}(x)} = \sum_{a=1}^{N-1}\sum_{b=a+1}^{N}\frac{\partial \Phi}{\partial r_{ab}}\int_0^1 \frac{\frac{\mathrm{d}x^i}{\mathrm{d}\lambda}\frac{\mathrm{d}x^j}{\mathrm{d}\lambda}}{2\sqrt{g_{ij}(\lambda)\frac{\mathrm{d}x^i}{\mathrm{d}\lambda}\frac{\mathrm{d}x^j}{\mathrm{d}\lambda}}}\,\mathrm{d}\lambda. \tag{5.18}$$

Changing back to Cartesian coordinates, we get

$$\frac{\delta \Phi}{\delta g_{ij}(x)} = \frac{1}{2}\sum_{a=1}^{N-1}\sum_{b=a+1}^{N}\frac{\partial \Phi}{\partial r_{ab}}\frac{r_{ab}^i r_{ab}^j}{r_{ab}}\int_0^1 \delta(\mathbf{r} - (1-\lambda)\mathbf{r}_a - \lambda\mathbf{r}_b)\,\mathrm{d}\lambda. \tag{5.19}$$

Finally, one finds

$$\begin{aligned} P^{ij}(\mathbf{r}) = &\left\langle \sum_{n=1}^{N}\frac{p_n^i p_n^j}{m_n}\delta(\mathbf{r} - \mathbf{r}_n)\right\rangle \\ &- \left\langle \sum_{a=1}^{N-1}\sum_{b=a+1}^{N}\frac{\partial \Phi}{\partial r_{ab}}\frac{r_{ab}^i r_{ab}^j}{r_{ab}}\int_0^1 \delta(\mathbf{r} - (1-\lambda)\mathbf{r}_a - \lambda\mathbf{r}_b)\,\mathrm{d}\lambda\right\rangle, \end{aligned} \tag{5.20}$$

where p_n^i is used to denote the ith component of the nth particle's momentum to adhere to the conventional notation. We notice that the contour of the integral is rigorously defined. This is to be contrasted with the equation found in Ref. [22].

5.2.2 Numerical Computation

We shall now turn to a more computationally inspired point of view, namely the discretization of the pressure tensor. We follow the paper by Goetz & Lipowsky [63] in deriving the formulae. The computation of the kinetic contribution to the stress tensor is a simple task, whereas the discretization of the configurational part is not quite as straightforward.

Again using the multidimensional scaling argument, we may transform the interparticle potential from a function of pairs to a function of positions. We then recognize the fact that the interparticle potential Φ can be divided into two-body, three-body and many-body potentials:

$$\Phi(\{\mathbf{r}_i(t)\}) = \sum_m U^{(m)}(\{\mathbf{r}_i(t)\}) = \sum_m \sum_{\langle j \rangle_m} U^{(m)}(\mathbf{r}_{j_1}, \ldots, \mathbf{r}_{j_m}), \tag{5.21}$$

where $U^{(m)}$ denotes the m-body potential. The summation over $\langle j \rangle_m$ is called a cluster sum and is defined to avoid double counting as

$$\sum_{\langle j \rangle_m} = \sum_{j_1 < \cdots < j_m} . \tag{5.22}$$

Now the configurational contribution to the pressure tensor arising from m-body interactions is given by

$$\sigma_C^{ab}(\mathbf{R}, t)^{(m)} = \sum_{k=1}^{m} \sum_{\langle j \rangle_m} \left[\nabla_{\mathbf{r}_{j_k}} U^{(m)}(\mathbf{r}_{j_1}, \ldots, \mathbf{r}_{j_m})\right]^a \int_{C_{j_l j_k}} \delta(\mathbf{R} - \mathbf{l}) \, \mathrm{d}l^b, \tag{5.23}$$

We may now average over all l's to get a more symmetric expression,

$$\sigma_C^{ab}(\mathbf{R}, t)^{(m)} = \frac{1}{m} \sum_{l=1}^{m} \sum_{k=1}^{m} \sum_{\langle j \rangle_m} \left[\nabla_{\mathbf{r}_{j_k}} U^{(m)}(\mathbf{r}_{j_1}, \ldots, \mathbf{r}_{j_m})\right]^a \int_{C_{j_l j_k}} \delta(\mathbf{R} - \mathbf{l}) \, \mathrm{d}l^b. \tag{5.24}$$

We also choose the contours $C_{j_l j_k}$ and $C_{j_k j_l}$ to be identical apart from their orientation. Thus,

$$\begin{aligned} \sigma_C^{ab}(\mathbf{R}, t)^{(m)} = \frac{1}{m} \sum_{l=1}^{m} \sum_{k=1}^{l-1} \sum_{\langle j \rangle_m} \Big(&\left[\nabla_{\mathbf{r}_{j_k}} U^{(m)}(\mathbf{r}_{j_1}, \ldots, \mathbf{r}_{j_m})\right]^a \\ &- \left[\nabla_{\mathbf{r}_{j_l}} U^{(m)}(\mathbf{r}_{j_1}, \ldots, \mathbf{r}_{j_m})\right]^a \Big) \int_{C_{j_l j_k}} \delta(\mathbf{R} - \mathbf{l}) \, \mathrm{d}l^b. \end{aligned} \tag{5.25}$$

In the literature, this is often written with cluster sums,

$$\begin{aligned}\sigma_C^{ab}(\mathbf{R},t)^{(m)} = \frac{1}{m}\sum_{\langle k\rangle_2}\sum_{\langle j\rangle_m}\Big(\Big[\nabla_{\mathbf{r}_{j_{k_1}}}U^{(m)}(\mathbf{r}_{j_1},\ldots,\mathbf{r}_{j_m})\Big]^a \\ -\Big[\nabla_{\mathbf{r}_{j_{k_2}}}U^{(m)}(\mathbf{r}_{j_1},\ldots,\mathbf{r}_{j_m})\Big]^a\Big)\int_{C_{j_{k_2}j_{k_1}}}\delta(\mathbf{R}-\mathbf{l})\,\mathrm{d}l^b.\end{aligned} \tag{5.26}$$

Note that the first sum goes from 1 to m, whereas the second one is a sum over the particles.

Next, we turn our attention to discretizing the integral of the delta distribution. We subdivide the simulation box into small cubes of volume V and calculate the average pressure tensor in each of these cubes, i.e. $P^{ab}(\mathbf{R}) = \int_V P^{ab}(\mathbf{R})\,\mathrm{d}^3\mathbf{R}/V$. We make the choice of IK contour, i.e. we choose the integration contours to be linear and parametrize them as

$$l^b = r^b_{j_{k_2}} + \lambda\left(r^b_{j_{k_1}} - r^b_{j_{k_2}}\right) = r^b_{j_{k_2}} + \lambda r^b_{j_{k_2}j_{k_1}},\ \text{with } \lambda\in[0,1]. \tag{5.27}$$

It follows that

$$\int_{C_{j_{k_2}j_{k_1}}}\delta(\mathbf{R}-\mathbf{l})\,\mathrm{d}l^b = -\int_0^1\delta\left(\mathbf{R}-\left(\mathbf{r}_{j_{k_2}}+\lambda\mathbf{r}_{j_{k_2}j_{k_1}}\right)\right)r^b_{j_{k_2}j_{k_1}}\,\mathrm{d}\lambda, \tag{5.28}$$

whose volumetric integral we discretize into N parts as

$$\int_V\int_{C_{j_{k_2}j_{k_1}}}\delta(\mathbf{R}-\mathbf{l})\,\mathrm{d}l^b\,\mathrm{d}^3\mathbf{R} \approx -\frac{r^b_{j_{k_2}j_{k_1}}}{N+1}\sum_{\lambda=0}^{N}f_V\left(\mathbf{r}_{j_{k_2}}+\frac{\lambda}{N}\mathbf{r}_{j_{k_2}j_{k_1}}\right), \tag{5.29}$$

where $f_V(\mathbf{R}) = 1$, if $\mathbf{R}\in V$, and zero otherwise.

Finally, we have a computationally tractable formula for the pressure tensor, namely

$$\begin{aligned}P^{ab}(\mathbf{R}) = \Bigg\langle\frac{1}{V}\sum_i m_i v_i^a v_i^b + \sum_m\frac{1}{mV}\sum_{\langle k\rangle_2}\sum_{\langle j\rangle_m}\Big(\Big[\nabla_{\mathbf{r}_{j_{k_1}}}U^{(m)}(\mathbf{r}_{j_1},\ldots,\mathbf{r}_{j_m})\Big]^a \\ -\Big[\nabla_{\mathbf{r}_{j_{k_2}}}U^{(m)}(\mathbf{r}_{j_1},\ldots,\mathbf{r}_{j_m})\Big]^a\Big)\frac{r^b_{j_{k_2}j_{k_1}}}{N+1}\sum_{\lambda=0}^{N}f_V\left(\mathbf{r}_{j_{k_2}}+\frac{\lambda}{N}\mathbf{r}_{j_{k_2}j_{k_1}}\right)\Bigg\rangle.\end{aligned} \tag{5.30}$$

Surface Tension

To compute the tensor above, we obviously need the positions and velocities of each particle at each time step. To get spatial resolution, we divide the simulation box into a grid, with each point of a volume V. A rectangular Cartesian tensor is not of great interest if we wish to analyze spherical systems. We therefore transform the calculated Cartesian tensor into a physical spherical basis, as outlined in Appendix 1. Finally,

we integrate out the angular degrees of freedom by taking statistical averages and get curves similar to those in Fig. 3.2. From here it is a trivial task, employing Eqs. (3.23) and (3.24) to calculate the surface tension. Due to numerical instabilities caused by insufficient sampling at the center of the coordinate system, highly fluctuating values of the pressure tensor around $r = 0$ are assumed to have the bulk pressure and thus drop from all integrals.

6. SYSTEMS STUDIED

The goal of this study is to understand the physical properties determining the fusion tendency of lipoprotein particles and how this broad issue is affected when the surface composition of the particles is modified. Due to the large computational demand of LDL particles, we opted for HDL as the reference system. In this initial study our model did not contain the protein, since it would make the analysis much more complicated and the computational load heavier. In other respects, the model was identical to that of [64], which was later published in Ref. [49]. Due to the way the particles are simulated on a computer and due to the fact that the exact composition varies, the microscopic details between different lipids are ignored and they are effectively described by POPC, lysoPC, cholesterol, cholesterol ester and trioleate.

To study the fusion tendencies, we resorted to gently pulling two such particles together, for spontaneous fusion would be too rare an event to simulate using non-steered MD. From the acquired data, we calculated an approximation for the rate of facilitated fusion. Finally, we altered the surface composition of the HDL droplet allthewhile trying to keep the surface tension constant to estimate the effects of different physical quantities, such as spontaneous curvature, since it is expected that the latter should have an effect on fusion tendencies, as detailed in earlier Chapters. As it is very difficult to calculate numerical values for these elastic quantities, especially spontaneous curvature, we changed the number of lysoPC molecules, which is known to have an effect of increasing spontaneous curvature in many systems.

As a control group, particles of extremely high surface tension were also simulated and a significant change in the rate of fusion was observed. A more modest modification was also performed and a change in the fusion rate was again recorded.

The exact numbers of constituents of each system are listed in Table 6.1.

A harmonic potential was used to pull the particles together. Each system was pulled 10 times, each time with a different starting configuration, which before the steered MD, energies were minimized using steepest descent and a 10 nm equilibriation MD was used. The fusion was defined to have occured when the cores of the particles were closer than 7 nm from each other, i.e. when the pulling force turned to be repulsive. At that moment the simulations were stopped.

Lipids	System			
	Ref. HDL	HDL core	Chol. → lysoPC	POPC → lysoPC
POPC	260	—	260	—
lysoPC	10	10	59	270
Chol.	49	49	—	49
Chol. Es.	122	122	122	122
Triol.	39	39	39	39

Table 6.1: Numbers of lipids in the studied systems.

All the simulations used the Nosé–Hoover thermostat and the Parrinello–Rahman barostat.

6.1 Reference HDL

By reference HDL we mean the model described in [49, 64] without the protein. This model is based on measurements of actual HDL extracted from humans. For simplicity we do not study fusion between particles containing proteins in this work. Our goal is to study which factors determine the fusion rate if it happens via monolayer contact, and taking out the protein does not significantly change the surface tension of the particle [65].

6.2 HDL Core

As a first test case or as a proof of concept, we simulated the fusion of two HDL cores. By HDL core, we mean the reference HDL stripped of its main surfactant, POPC. As shown in [65], removal of surfactants results in an increase of surface tension, as expected. Therefore, the fusion of such particles should be much faster, practically instantaneous. Due to the failure of the model of Ref. [4] in a similar setting, this is an important test of model verification.

6.3 Cholesterol → lysoPC

Next, we prepared a system with all the cholesterol particles of the reference HDL changed to lysoPC. The motivation of this change is that lysoPC has a large head group and just one tail. As such, increasing the amount of lysoPC should change the spontaneous curvature towards the positive direction. Cholesterol on the other hand has a rather small head group and a large tail, and therefore probably acts to decrease the spontaneous curvature.

Such a change, however, modifies all of the other elastic properties as well. Cholesterol is usually associated with rigid membranes as it tends to order the lipids around it [66]. With the bending modulus k changing, one can assume that

the Gaussian bending modulus $\bar{k}$ does not stay constant either. Furthermore, as cholesterol is not as strong a surfactant as lysoPC, we expect that by changing the composition as described, we lower the surface tension.

All in all, lower surface tension means slower fusion. A more positive spontaneous curvature is expected to slow down the fusion as well. However, decreasing k and $\bar{k}$ ought to accelerate the fusion rate. Because of the competing effects, it is difficult to predict whether replacing cholesterol by lysoPC induces or inhibits fusion.

6.4 POPC → lysoPC

Because the proposed fusion mechanism relies on the flip-flop of tails, it is plausible the the amount of tails would affect the fusion tendency. This is why we constructed a rather extreme system by changing all of the reference HDL's POPC molecules to lysoPC. As lysoPC does not quite cover as much area as POPC, we expected a rise in surface tension. The matter is not quite this simple though, because the part that was removed from POPC is largely hydrophobic.

7. RESULTS AND DISCUSSION

In this Chapter we briefly go though the main results of this Thesis. In addition to the results from numerical simulations, highlighted in this Chapter, much of this Thesis was devoted to reviewing the theory behind fusion and shall thus be quickly revisited.

7.1 Theoretical Derivations

In this Thesis well known theoretical results were reviewed in a consistent fashion with their full derivations, not typically found in the literature. Furthermore, less well known results were presented, again with full derivations, putting the pressure tensor formalism on a more solid ground, where we may now consider it, at least qualitatively, as a useful quantity. The most important of these is the claim of Ref. [20], where the pressure tensor, as the functional derivative of the free energy with respect to the metric tensor, was shown to be unique, and of the form of Eqs. (5.20) and (5.30), which are used in all the calculations of the pressure tensor. If one restricts the variation to the Cartesian metric, gauge arbitrariness is introduced [57], and problems of the traditional treatment arise [22].

Although we provided the thermodynamical foundations of interfacial tension in Chapter 3.1, we consider the quantity largely from a mechanical standpoint, as in Chapter 3.3, leading to Eqs. (3.23) and (3.24), which, used extensively in the next Section, connect the pressure tensor to surface tension.

We furthermore attempted at a generalization of the model of Ref. [38] to lipoprotein droplets by assuming any created voids would be filled by the hydrophobic core. The resulting highly nonlinear set of differential equations could not be linearized as done in Ref. [38] and proved difficult to solve using standard mixed self-consistent numerical solution methods.

7.2 Simulation Results

Table 7.1 summarizes our numerical results, followed by a more in-depth analysis and discussion below. Also depicted is the time dependence of the pulling force between the two fusing particles as fusion takes place (Fig. 7.1) and the same event visualized (Fig. 7.2).

	Ref. HDL	HDL core	Chol. → lysoPC	POPC → lysoPC
Fusion time (ns)	133 ± 30	instantaneous	193 ± 30	$\gg 500$
Surf. ten. (mN/m)	25 ± 2	41 ± 2	23 ± 2	28 ± 2

Table 7.1: Results for the fusion time and surface tension.

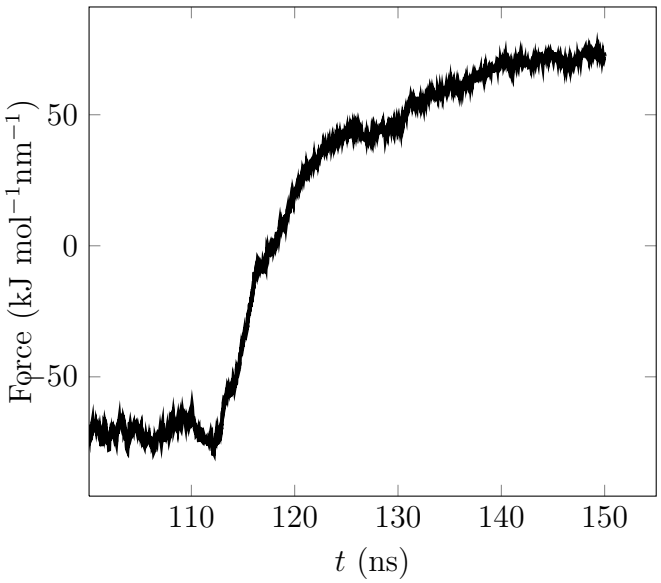

Figure 7.1: An example of a fusion event. Shown is the pulling force between two particles. Before the event ($t < 100$ ns) the force stays relatively constant (not shown) and rapidly changes as fusion takes place. The simulation was stopped at $t = 150$ ns.

7.3 Effect of Surface Tension

As the effect of surface tension is to minimize interfacial area between two phases, it is intuitive that due to phase separation, two spheres should merge to form one and that the higher the surface tension, the higher the urge to do so. Indeed, we see this trend in our simulations: HDL core fuses much faster than the reference HDL while the Cholesterol → lysoPC system fuses slower. From the change in surface tension, both of these results are quite expected, but previous models have been unable to reproduce them [4]. However, unexpected behaviour is found in the case of POPC → lysoPC system: the interfacial tension is higher compared to the reference but the fusion rate is significantly slower.

7.4 Effect of Curvature

As already mentioned, the POPC → lysoPC system makes an important exception to the rule, as although its surface tension is higher than that of the reference HDL, it has a slower rate of fusion. There are several ways to explain this discrepancy. Assuming that the stalk formation is indeed the rate limiting step, the fusion process ought to be slower if either the bending modulus or the spontaneous curvature is

increased. When changing POPC to lysoPC, both arguments are likely valid, for lysoPC has a smaller tail, so it can pack more rigidly. Also because of the smaller tail, it has a larger head group to tail size ratio, which means that it has a more positive spontaneous curvature.

7.5 Other Considerations

However, it has been suggested that stalk formation is not the rate limiting step of fusion and there is some computational evidence to support this argument. Kinnunen [34] argues that the fusion process is sparked by a single two-tailed lipid, when one of its tails flip-flops into the other particle. If one introduces a lipid with one tail in one HDL and the other in another HDL, fusion happens instantaneously. Therefore one might argue that changing POPC to lysoPC also alters the whole fusion mechanism and that the mechanism is so microscopic that it cannot be captured by a continuum theory. Therefore the system POPC $\rightarrow$ lysoPC, according to the reasoning above, should be compared to POPC rich systems with care.

We found individual events favoring the idea of lipid tail induced fusion (see Fig. 7.3), indicating that stalk formation might not be the rate limiting step, but instead the flipping of tails might be. Further work into this direction is planned, such as determining the free energies of pulling lipid tails out of a monolayer as a function of membrane lipid composition.

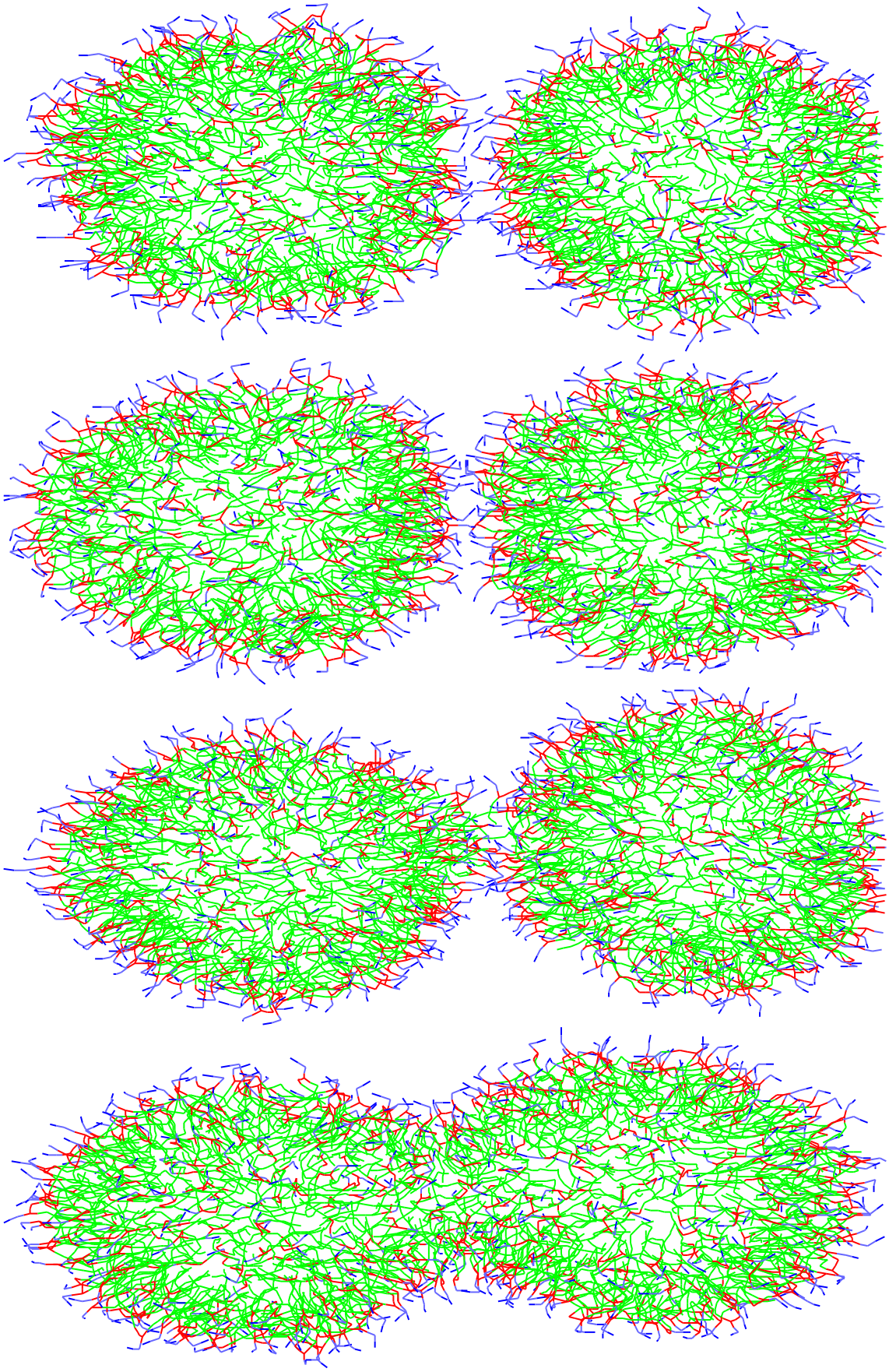

Figure 7.2: An example of a fusion event. From top to bottom, shown are snapshots of the system at times $t = 100$ ns, $t = 110$ ns, $t = 112.5$ ns, and $t = 115$ ns, respectively.

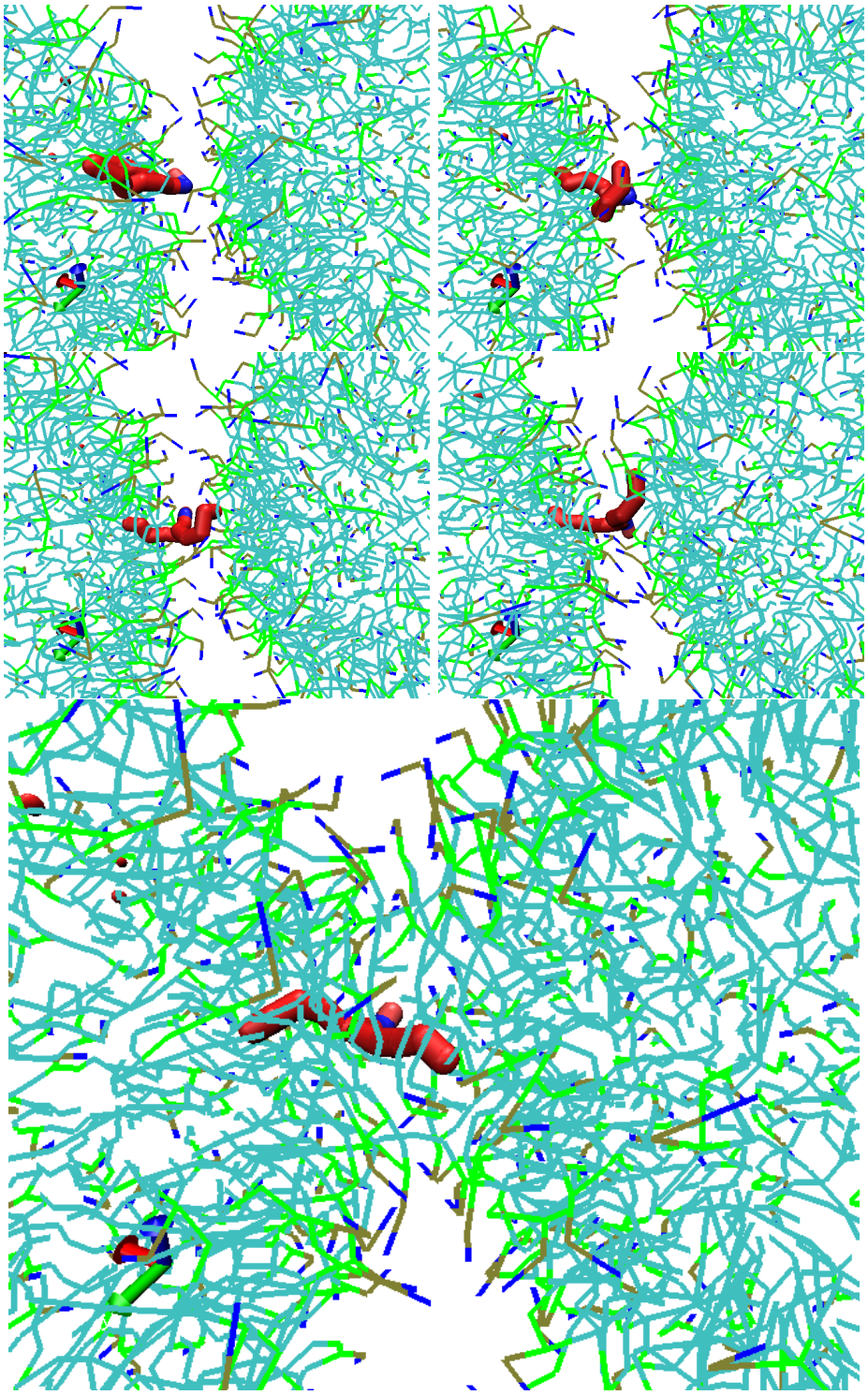

Figure 7.3: A closer look of a fusion event. Shown is a highlighted POPC molecule which seems to trigger the fusion, at times (from left to right, top to bottom) $t = 111$ ns, $t = 111.5$ ns, $t = 112$ ns, $t = 112.5$ ns and $t = 113$ ns (large image), respectively.

8. CONCLUSIONS AND FUTURE WORK

In this Thesis we have developed a method to study relative fusion rates of lipid droplets with varying surface compositions. Furthermore, we have combined this method with surface tension calculations to enable the study of correlation between fusion rate and surface tension.

We have demonstrated that by changing the surface composition of particles similar to lipoproteins in a way feasible in a laboratory, the shift in fusion tendency cannot be explained simply by surface tension. Alternative explanations, such as curvature effects and a different fusion mechanism, were provided, but further work into this direction is suggested. The fusion mechanism could be studied by calculating free energies of pulling lipid tails out of the membrane as a function of membrane lipid composition. The fusion tendency of lipids with several tails, but with a comparable spontaneous curvature to those with one tail should be tried out. If a system with a large positive curvature, comparable to lysoPC, would fuse, this would indicate the need of several tails to induce fusion.

We have further developed a model that, unlike previous models, correctly reproduces the fusion of highly hydrophobic particles in the lack of a surfactant. This would suggest the level of detail of the present model is such that it captures the essentials of the fusion process.

In the future, the methods developed as a part of this Thesis may be applied to study the fusion mechanism and tendencies of biologically relevant particle modifications.

The recent treatment of Refs. [60, 61] of pressure tensors has received very little attention. As they suggest a new, simpler, unique, local form for pressure tensor when the interactions are of short range, their formalism should be tried out numerically. They caution the usage of pressure tensors in systems with long range interactions. Coarse-grained force fields, such as the MARTINI force field employed in this Thesis have been said to reproduce required smoothness properties better than all-atom parametrizations: For example the mechanical stability condition of Eq. (3.42) is often violated, but this is usually claimed to be due to numerical errors, insufficient sampling or constraint forces, as it seems certain molecules with constraint force fields amplify the effect. We, however, propose that as the MARTINI model uses cut-offs, this might be a factor in suppressing oscillations. We suggest future studies into

this matter by computing and comparing the traditional Irving–Kirkwood pressure tensor and that of Ref. [61] to verify the quantitative foundations of the pressure tensor program.

BIBLIOGRAPHY

[1] V. Kumar, A. K. Abbas, N. Fausto, & Mitchell R. *Robbins Basic Pathology*. Elsevier, 8 edition, 2007.

[2] J. K. Hakala, K. Öörni, M. Ala-Korpela, & P. T. Kovanen. Lipolytic Modification of LDL by Phospholipase A2 Induces Particle Aggregation in the Absence and Fusion in the Presence of Heparin. *Arterioscler. Thromb. Vasc. Biol.*, **19**:1276–1283, 1999.

[3] V. S. Markin, M. M. Kozlov, & V. L. Borovjagin. On the Theory of Membrane Fusion: The Stalk Mechanism. *Gen. Physiol. Biophys.*, **3**:361–377, 1984.

[4] L. Rekvig & D. Frenkel. Molecular Simulations of Droplet Coalescence in Oil/Water/Surfactant Systems. *J. Chem. Phys.*, **127**:134701, 2007.

[5] J. Moore & R. Langley. *Biochemistry for Dummies*. Wiley, 2008.

[6] S. A. Safran. *Statistical Thermodynamics of Surfaces, Interfaces, and Membranes*. Addison–Wesley, 1994.

[7] T. L. Hill. Statistical Thermodynamics of the Transition Region Between Two Phases. I. Thermodynamics and Quasi-Thermodynamics. *J. Phys. Chem.*, **56**:526–531, 1952.

[8] S. Kondo. Thermodynamical Fundamental Equation for Spherical Interface. *J. Chem. Phys.*, **25**:662–669, 1956.

[9] O. H. S. Ollila & I. Vattulainen. Lateral Pressure Profiles in Lipid Membranes: Dependence on Molecular Composition. In M. S. P. Sansom & P. C. Biggin, editors, *Molecular Simulations and Biomembranes: From Biophysics to Function*. Royal Society of Chemistry, 2010.

[10] R. S. Cantor. Lateral Pressures in Cell Membranes: A Mechanism for Modulation of Protein Function. *J. Phys. Chem. B*, **101**:1723–1725, 1997.

[11] R. S. Cantor. The Lateral Pressure Profile in Membranes: A Physical Mechanism of General Anesthesia. *Toxicol. Lett.*, **100**:451–458, 1998.

[12] R. S. Cantor. Lipid Composition and the Lateral Pressure Profile in Bilayers. *Biophys. J.*, **76**:2625–2639, 1999.

[13] H. El Bardouni, M. Mareschal, R. Lovett, & M. Baus. Computer Simulation Study of the Local Pressure in a Spherical Liquid–Vapor Interface. *J. Chem. Phys.*, **113**:9804, 2000.

[14] S. Chen, G. D. Doolen, & K. G. Eggert. Lattice-Boltzmann Fluid Dynamics: A Versatile Tool for Multiphase and Other Complicated Flows. *Los Alamos Science*, **22**:99–111, 1994.

[15] S. I. Mukhin & S. Baoukina. Analytical Derivation of Thermodynamic Characteristics of Lipid Bilayer from a Flexible String Model. *Phys. Rev. E*, **71**: 061918, 2005.

[16] A. Ben-Shaul. Chapter 7: Molecular Theory of Chain Packing, Elasticity and Lipid-Protein Interaction in Lipid Bilayers. In R. Lipowsky & E. Sackmann, editors, *Handbook of Biological Physics, Volume 1, Part 1*. Elsevier, 1995.

[17] J. S. Rowlinson & B. Widom. *Molecular Theory of Capillarity*. Dover, 2nd edition, 2002.

[18] F. P. Buff. Spherical Interface. II. Molecular Theory. *J. Chem. Phys.*, **23**: 419–426, 1955.

[19] P. A. Kralchevsky & K. Nagayama. *Particles at Fluid Interfaces and Membranes*. Elsevier, 2001.

[20] L. Mistura. The Pressure Tensor in Nonuniform Fluids. *J. Chem. Phys.*, **83**: 3633–3637, 1985.

[21] L. Mistura. The Definition of the Pressure Tensor in the Statistical Mechanics of Nonuniform Classical Fluids. *Int. J. Thermophys.*, **8**:397–403, 1987.

[22] P. Schofield & J. R. Henderson. Statistical Mechanics of Inhomogeneous Fluids. *Proc. R. Soc. Lond. A*, **379**:231–246, 1982.

[23] M. Baus & R. Lovett. The Magnitude and Location of the Surface Tension of Curved Surfaces. *J. Chem. Phys.*, **103**:377–392, 1995.

[24] R. Lovett & M. Baus. A Molecular Theory of the Laplace Relation and of the Local Forces in a Curved Interface. *J. Chem. Phys.*, **106**:635–644, 1997.

[25] P. M. Chaikin & T. C. Lubensky. *Principles of Condensed Matter Physics*. Cambridge, 2000.

[26] W. Helfrich. Elastic Properties of Lipid Bilayers: Theory and Possible Experiments. *Z. Naturforsch.*, **28**:693–703, 1973.

[27] J. H. Weiner. *Statistical Mechanics of Elasticity.* Dover, 2002.

[28] A. H. Nayfeh. *Introduction to Perturbation Techniques.* Wiley, 1981.

[29] H. Hammarén. Private communications, Tampere, 2009.

[30] E. M. Blokhuis & D. Bedeaux. Pressure Tensor of a Spherical Interface. *J. Chem. Phys*, **97**:3576, 1992.

[31] R. C. Tolman. The Effect of Droplet Size on Surface Tension. *J. Chem. Phys.*, **17**:333–337, 1949.

[32] A. J. Markvoort & S. J. Marrink. Chapter 11: Lipid Acrobatics in the Membrane Fusion Arena. In L. V. Chernomordik & M. M. Kozlov, editors, *Current Topics in Membranes, Volume 68.* Elsevier, 2011.

[33] K. Katsov, M. Müller, & M. Schick. Field Theoretic Study of Bilayer Membrane Fusion. I. Hemifusion Mechanism. *Biophys. J.*, **87**:3277–3290, 2004.

[34] P. K. J. Kinnunen. Fusion of Lipid Bilayers: A Model Involving Mechanistic Connection to H_{II} Phase Forming Lipids. *Chem. Phys. Lipids*, **63**:251–258, 1992.

[35] J. S. Marrink & A. E. Mark. The Mechanism of Vesicle Fusion as Revealed by Molecular Dynamics Simulations. *J. Am. Chem. Soc.*, **125**:11144–11145, 2003.

[36] V. S. Markin & J. P. Albanesi. Membrane Fusion: Stalk Model Revisited. *Biophys. J*, **82**:693–712, 2002.

[37] Y. Kozlovsky & M. M. Kozlov. Stalk Model of Membrane Fusion: Solution of Energy Crisis. *Biophys. J.*, **82**:882–895, 2002.

[38] S. May. Structure and Energy of Fusion Stalks: The Role of Membrane Edges. *Biophys. J.*, **83**:2969–2980, 2002.

[39] D. P. Siegel. The Gaussian Curvature Elastic Energy of Intermediates in Membrane Fusion. *Biophys. J.*, **95**:5200–5215, 2008.

[40] A. Kabalnov & H. Wennerstrom. Macroemulsion Stability: The Oriented Wedge Theory Revisited. *Langmuir*, **12**:276–292, 1996.

[41] D. C. Rapaport. *The Art of Molecular Dynamics Simulation.* Cambridge, 2nd edition, 2004.

[42] R. Car & M. Parrinello. Unified Approach for Molecular Dynamics and Density-Functional Theory. *Phys. Rev. Lett.*, **55**:2471–2474, 1985.

[43] J. M. Thijssen. *Computational Physics*. Cambridge, 2nd edition, 2007.

[44] B. Hess, C. Kutzner, D. van der Spoel, & E. Lindahl. GROMACS 4: Algorithms for Highly Efficient, Load-Balanced, and Scalable Molecular Simulation. *J. Chem. Theory Comput.*, **4**:435–447, 2008.

[45] A. R. Leach. *Molecular Modelling: Principles and Applications*. Pearson, 2nd edition, 2001.

[46] S. J. Marrink, A. H. de Vries, & A. E. Mark. Coarse Grained Model for Semiquantitative Lipid Simulations. *J. Phys. Chem. B*, **108**:750–760, 2004.

[47] S. J. Marrink, H. J. Risselada, S. Yefimov, D. P. Tieleman, & A. H. de Vries. The MARTINI Force Field: Coarse Grained Model for Biomolecular Simulations. *J. Phys. Chem. B*, **111**:7812–7824, 2007.

[48] J. N. Israelachvili. *Intermolecular and Surface Forces*. Elsevier, 2nd edition, 1991.

[49] T. Vuorela, A. Catte, P. S. Niemelä, A. Hall, M. T. Hyvönen, S. J. Marrink, M. Karttunen, & I. Vattulainen. Role of Lipids in Spheroidal High Density Lipoproteins. *PLoS Comput. Biol.*, **6**:e1000964, 10 2010.

[50] S. J. Marrink, M. Fuhrmans, J. Rissedala, & X. Periole. Chapter 2: The MARTINI Forcefield. In G. Voth, editor, *Coarse Graining of Condensed Phase and Biomolecular Systems*. CRC Press, 2008.

[51] K. Glavatskiy. *Multicomponent Interfacial Transport as Described by the Square Gradient Model; Evaporation and Condensation*. Ph.D. Thesis, Norwegian University of Science and Technology, 2009.

[52] E. Wajnryb, A. R. Altenberger, & J. S. Dahler. Uniqueness of the Microscopic Stress Tensor. *J. Chem. Phys.*, **103**:9782–9787, 1995.

[53] J. H. Irving & J. G. Kirkwood. The Statistical Mechanical Theory of Transport Processes. IV. The Equations of Hydrodynamics. *J. Chem. Phys.*, **18**:817–829, 1950.

[54] M. Mareschal, M. Baus, & R. Lovett. The Local Pressure in a Cylindrical Liquid–Vapor Interface: A Simulation Study. *J. Chem. Phys.*, **106**:645–654, 1997.

[55] A. Harasima. Molecular Theory of Surface Tension. *Adv. Chem. Phys*, **1**: 203–237, 1958.

[56] B. Hafskjold & T. Ikeshoji. Microscopic Pressure Tensor for Hard-Sphere Fluids. *Phys. Rev. E*, **66**:11203, 2002.

[57] C. L. Rogers & A. M. Rappe. Geometric Formulation of Quantum Stress Fields. *Phys. Rev. B*, **65**:224117, 2002.

[58] Hu Jian-Guo & Ou-Yang Zhong-Can. Shape Equations of the Axisymmetric Vesicles. *Phys. Rev. E*, **47**:461–467, 1993.

[59] F. Jülicher & U. Seifert. Shape Equations for Axisymmetric Vesicles: A Clarification. *Phys. Rev. E*, **49**:4728–4731, 1994.

[60] S. Morante, G. C. Rossi, & M. Testa. The Stress Tensor of a Molecular System: An Exercise in Statistical Mechanics. *J. Chem. Phys.*, **125**:034101, 2006.

[61] G. C. Rossi & M. Testa. The Stress Tensor in Thermodynamics and Statistical Mechanics. *J. Chem. Phys.*, **132**:074902, 2010.

[62] I. Borg & P. J. F. Groenen. *Modern Multidimensional Scaling: Theory and Applications*. Springer, 2005.

[63] R. Goetz & R. Lipowsky. Computer Simulations of Bilayer Membranes: Self-Assembly and Interfacial Tension. *J. Chem. Phys.*, **108**:7397, 1998.

[64] T. Vuorela. *Lipoprotein Droplets Modeled by Coarse Grained Molecular Dynamics Simulations*. Master's Thesis, Tampere University of Technology, 2007.

[65] M. Lehtivaara. *Lipoproteiinimallien pintajännityksen määrittäminen molekyylidynamiikkasimulaatioista*. Bachelor's Thesis, Tampere University of Technology, 2010.

[66] H. Martinez-Seara, T. Róg, M. Pasenkiewicz-Gierula, I. Vattulainen, M. Karttunen, & R. Reigada. Interplay of Unsaturated Phospholipids and Cholesterol in Membranes: Effect of the Double-Bond Position. *Biophys. J.*, **95**:3295–3305, 2008.

[67] G. B. Arfken & H. J. Weber. *Mathematical Methods for Physicists*. Elsevier, 6th edition, 2005.

[68] J. H. Heinbockel. *Introduction to Tensor Calculus and Continuum Mechanics*. Trafford, 2001.

APPENDIX 1: SPHERICAL COORDINATE SYSTEM

In this appendix, we shall briefly review the main properties of the spherical coordinate system (see Fig. A1.1). Much of the following discussion is applicable to more general curvilinear coordinates as well. In the course of this treatment, we make extensive use of the Einstein summation convention, i.e. we drop the summation signs Σ, and assume that repeated indices are summed over.

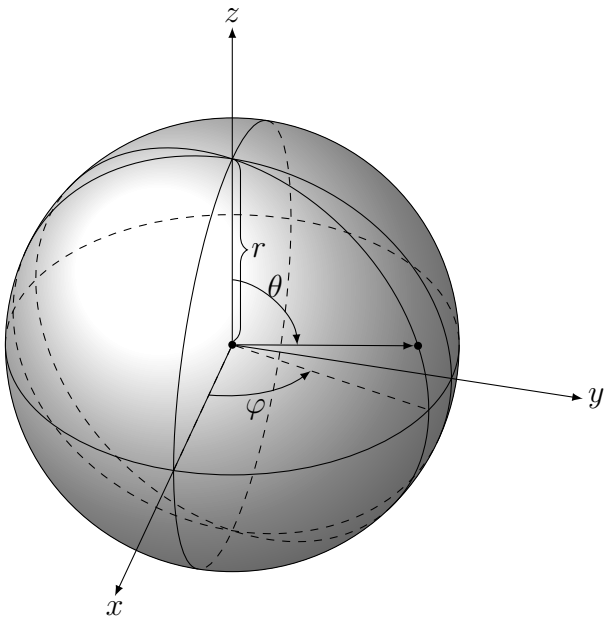

Figure A1.1: The spherical coordinate system: $x = r\cos\varphi\sin\theta$, $y = r\sin\varphi\sin\theta$, $z = r\cos\theta$

We shall also define curvature from an elementary viewpoint, as it is an important and a recurrent quantity throughout this Thesis.

1.1 A Primer on Tensors

The *metric tensor* g_{ij} is a function that describes the shape of the coordinate basis used. Let $\mathbf{r}(x^1, \ldots, x^n)$ be a parametrization of the n-dimensional space under consideration. The basis vectors in the *natural coordinate basis* are defined as $\mathbf{e}_i = \partial_i \mathbf{r}(x^1, \ldots, x^n)$, for $i = 1, \ldots, n$. From these one obtains the metric tensor:

$$g_{ij}(x^1, \ldots, x^n) = \mathbf{e}_i \cdot \mathbf{e}_j. \tag{A1.1}$$

The differential line element $\mathrm{d}s$ can be given with the help of the metric tensor as follows: $\mathrm{d}s^2 = g_{ij}\,\mathrm{d}x^i\,\mathrm{d}x^j$. For the Cartesian coordinate system, $g_{ij} = \delta_{ij}$, the Kronecker delta. We thus recover the Pythagorean theorem in Cartesian coordinates,

$\mathrm{d}s^2 = \mathrm{d}x^2 + \mathrm{d}y^2 + \mathrm{d}z^2$.

The natural coordinate basis for spherical coordinates is

$$[g_{ij}(r,\theta,\varphi)] = \begin{pmatrix} 1 & 0 & 0 \\ 0 & r^2 & 0 \\ 0 & 0 & r^2\sin^2\theta \end{pmatrix}, \tag{A1.2}$$

where the square brackets denote a matrix representation. In this basis, there is no tangential velocity, but rather the concept of angular velocity, which has different units (s^{-1} as opposed to m/s). The *physical coordinate basis* we define as the coordinate basis with unit basis vectors. This definition guarantees the normalization of units.

Tensor, from a physicist's point of view, is a coordinate invariant quantity and *vice versa*. Therefore, all physical quantities have a tensorial nature. Reviewing tensor calculus in all detail is out of scope of this Thesis (see e.g. [67, 68] for a more complete introduction at a level suitable for our purposes). We merely collect the relevant formulæ below accompanied by a short justification:

1. There are two types of tensors, namely covariant and contravariant tensors. A *covariant tensor* T_i of rank 1 obeys the following law of transformation upon a change of coordinates $x^i \to x^{i'}$ (Note the notation: Primed indices are not just different indices but refer to a different coordinate basis altogether):

$$T_{i'} = \frac{\partial x^i}{\partial x^{i'}} T_i. \tag{A1.3}$$

   Similarly, a rank 1 tensor S^i is *contravariant* if upon a change of variables,

$$S^{i'} = \frac{\partial x^{i'}}{\partial x^i} S^i. \tag{A1.4}$$

   These can be used to write out tensors of the mixed type, e.g. a rank (1,1) tensor P^i_j transforms as:

$$P^{i'}_{j'} = \frac{\partial x^{i'}}{\partial x^i}\frac{\partial x^j}{\partial x^{j'}} P^i_j. \tag{A1.5}$$

2. In our field of interest, covariant and contravariant tensors can be converted to one another through multiplication by the metric tensor or its inverse, e.g. $T_i = g_{ij}T^j$.

3. The transformation from the natural to the physical coordinate basis for a

general tensor $T^{i_1\ldots i_n}_{j_1\ldots j_m}$ is done as follows:

$$\hat{T}(i_1,\ldots,i_n,j_1,\ldots,j_m) = T^{i_1\ldots i_n}_{j_1\ldots j_m}\frac{\sqrt{g_{i_1i_1}}\cdots\sqrt{g_{i_ni_n}}}{\sqrt{g_{j_1j_1}}\cdots\sqrt{g_{j_mj_m}}} \quad \text{(no summations)}, \tag{A1.6}$$

where by the hatted $\hat{T}$ we indicate the physical components.

4. The electric field of a point charge is spherically symmetric. If we were to simply take the partial derivatives of the components of the vector field in the spherical coordinate system, the radial component would be the sole nonvanishing term. It is, however, intuitively clear, that the field is not "flat" and that it varies throughout space. Componentwise partial differentiation ignores the fact that the basis vectors change as a function of position, as can be readily confirmed by partial differentiation of the vector field itself:

$$\partial\mathbf{E} = \partial(E^i\mathbf{e}_i) = \partial(E^i)\mathbf{e}_i + E^i\partial(\mathbf{e}_i). \tag{A1.7}$$

The last term on the right is the correction factor that takes into account the change in the basis vectors. These terms are bundled up to form the so-called *Christoffel symbols* Γ^i_{jk}. The regular partial differentiation with respect to x^i we denote by the subscript "$,i$", for example

$$T_{i,j} = \frac{\partial T_i}{\partial x^j}. \tag{A1.8}$$

Finally we are ready to differentiate the components of a tensor field. For a rank 1 covariant tensor T_i, the *covariant derivative* is defined as follows:

$$T_{i;j} = T_{i,j} - \Gamma^k_{ij}T_k. \tag{A1.9}$$

Similarly, for a contravariant tensor $\mathbf{S}$,

$$S^{i;j} = S^i_{,j} + \Gamma^i_{kj}S^k. \tag{A1.10}$$

These can be combined for e.g. a rank (2,1) tensor P^{ij}_k,

$$P^{ij}_{k;l} = P^{ij}_{k,l} + \Gamma^i_{ml}P^{mj}_k + \Gamma^j_{ml}P^{im}_k - \Gamma^m_{kl}P^{ij}_m. \tag{A1.11}$$

Divergence is a contraction with the covariant derivative, e.g. $P^{ij}_{k;i}$.

5. The Christoffel symbols clearly depend on the derivatives of the metric (see

Eq. (A1.7)). In fact,

$$\Gamma^i_{jk} = \frac{1}{2} g^{im} \left(\frac{\partial g_{mj}}{\partial x^k} + \frac{\partial g_{mk}}{\partial x^j} - \frac{\partial g_{jk}}{\partial x^m} \right). \tag{A1.12}$$

One should note that the Christoffel symbols themselves do not transform as tensors.

Christoffel symbols for the spherical coordinate system, as defined by the metric tensor of Eq. (A1.2):

$$\mathbf{\Gamma}^r = \begin{pmatrix} 0 & 0 & 0 \\ 0 & -r\sin^2\theta & 0 \\ 0 & 0 & -r \end{pmatrix} \tag{A1.13}$$

$$\mathbf{\Gamma}^\theta = \begin{pmatrix} 0 & \frac{1}{r} & 0 \\ \frac{1}{r} & 0 & \frac{1}{\tan\theta} \\ 0 & \frac{1}{\tan\theta} & 0 \end{pmatrix} \tag{A1.14}$$

$$\mathbf{\Gamma}^\varphi = \begin{pmatrix} 0 & 0 & \frac{1}{r} \\ 0 & -\sin\theta\cos\theta & 0 \\ \frac{1}{r} & 0 & 0 \end{pmatrix} \tag{A1.15}$$

Integration of a scalar in spherical coordinates:

$$\int_{\Omega_c} f(x,y,z)\,\mathrm{d}x\,\mathrm{d}y\,\mathrm{d}z = \int_{\Omega_s} f(r,\theta,\varphi)\sqrt{g}\;\mathrm{d}r\,\mathrm{d}\theta\,\mathrm{d}\varphi, \tag{A1.16}$$

where g is the determinant of the metric and its square root acts as the Jacobian determinant of the substitution, as expected.

The transformation matrices from the Cartesian to the physical spherical coordinate system (length-preserving, and thus could be considered as rotation matrices):

$$\left[\frac{\partial x^{i'}}{\partial x^i}\right] = \left[\frac{\partial x^i}{\partial x^{i'}}\right]^{\mathrm{T}} = \begin{pmatrix} \sin\theta\cos\varphi & \sin\theta\sin\varphi & \cos\varphi \\ \cos\theta\cos\varphi & \cos\theta\sin\varphi & -\sin\varphi \\ -\sin\theta & \cos\theta & 0 \end{pmatrix} \tag{A1.17}$$

1.2 Curvature

To fully appreciate the mathematics of the stalk model of fusion, the notion of curvature must be defined with rigour. Although we have been using tensor calculus up to this point, we shall stick to a more elementary notation using vectors, as it is sufficient for our purposes.

Let $\mathbf{r}(u,v)$ be a parametrization of a surface. As the coordinates u, v move along the surface, $\mathbf{r}_u$ and $\mathbf{r}_v$ are the tangent vectors in the u and v directions, respectively.

It immediately follows that the unit normal may be written as

$$\mathbf{n} = \frac{\mathbf{r}_u \times \mathbf{r}_v}{\|\mathbf{r}_u \times \mathbf{r}_v\|}, \tag{A1.18}$$

where, adhering to convention, $\mathbf{r}_u$ denotes the common partial derivative with respect to u. We may now define the second fundamental form II, which describes curvature as a matrix:

$$\mathrm{II} = \begin{pmatrix} \mathbf{r}_{uu} \cdot \mathbf{n} & \mathbf{r}_{vu} \cdot \mathbf{n} \\ \mathbf{r}_{uv} \cdot \mathbf{n} & \mathbf{r}_{vv} \cdot \mathbf{n} \end{pmatrix}. \tag{A1.19}$$

The eigenvalues of II are called the principal curvatures. Their mean is called the mean curvature, and their product the Gaussian curvature. Informally speaking, the derivatives of the tangent vectors describe curvature in the sense of a second order fit of a circle. Thus the curvature of a sphere is the reciprocal of its radius.